NeuroImage 122 (2015) 355–372

Contents lists available at ScienceDirect

NeuroImage

journal homepage: www.elsevier.com/locate/ynimg

Physiologically informed dynamic causal modeling of fMRI data

Martin Havlicek [a,1,2,3], Alard Roebroeck [a], Karl Friston [b], Anna Gardumi [a], Dimo Ivanov [a], Kamil Uludag [a]

[a] Dept. of Cognitive Neuroscience, Maastricht University, 6200MD Maastricht, The Netherlands
[b] Wellcome Trust Centre for Neuroimaging, Institute of Neurology, University College London, London WC1N 3BG, United Kingdom

ARTICLE INFO

Article history:
Received 9 January 2015
Accepted 28 July 2015
Available online 5 August 2015

Keywords:
Hemodynamic model
Feedforward neurovascular coupling
Dynamic causal modeling (DCM)
BOLD signal
Excitation–inhibition
Post-stimulus undershoot

ABSTRACT

The functional MRI (fMRI) signal is an indirect measure of neuronal activity. In order to deconvolve the neuronal activity from the experimental fMRI data, biophysical generative models have been proposed describing the link between neuronal activity and the cerebral blood flow (the neurovascular coupling), and further the hemodynamic response and the BOLD signal equation. These generative models have been employed both for single brain area deconvolution and to infer effective connectivity in networks of multiple brain areas. In the current paper, we introduce a new fMRI model inspired by experimental observations about the physiological underpinnings of the BOLD signal and compare it with the generative models currently used in dynamic causal modeling (DCM), a widely used framework to study effective connectivity in the brain. We consider three fundamental aspects of such generative models for fMRI: (i) an adaptive two-state neuronal model that accounts for a wide repertoire of neuronal responses during and after stimulation; (ii) feedforward neurovascular coupling that links neuronal activity to blood flow; and (iii) a balloon model that can account for vascular uncoupling between the blood flow and the blood volume. Finally, we adjust the parameterization of the BOLD signal equation for different magnetic field strengths. This paper focuses on the form, motivation and phenomenology of DCMs for fMRI and the characteristics of the various models are demonstrated using simulations. These simulations emphasize a more accurate modeling of the transient BOLD responses — such as adaptive decreases to sustained inputs during stimulation and the post-stimulus undershoot. In addition, we demonstrate using experimental data that it is necessary to take into account both neuronal and vascular transients to accurately model the signal dynamics of fMRI data. By refining the models of the transient responses, we provide a more informed perspective on the underlying neuronal process and offer new ways of inferring changes in local neuronal activity and effective connectivity from fMRI.

Introduction

Functional magnetic resonance imaging (fMRI) is a widely employed non-invasive technique to assess brain function with unprecedented spatial and temporal resolution. However, fMRI signal reflects neuronal activity only indirectly, through the measurements of accompanying hemodynamic processes. An increase in neuronal activity causes localized changes in the cerebral metabolic rate of oxygen metabolism ($CMRO_2$), the cerebral blood flow (CBF), and the cerebral blood volume (CBV). As a result, the oxygen extraction fraction (E) (i.e. the blood oxygen saturation and the concentration of deoxygenated hemoglobin) changes, which is reflected in the blood oxygenation level-dependent (BOLD) signal.[4] Therefore, knowing the causal chain of these physiological processes is important to allow deducing the neuronal activity from experimental fMRI data (Roebroeck et al., 2011; Valdes-Sosa et al., 2011). As a result, a number of generative models of the fMRI signal have been proposed during the last two decades (e.g. Friston et al. (2000); Sotero and Trujillo-Barreto (2007), and Buxton et al. (2004)).

A prominent methodological framework that models the biophysical processes linking neuronal activity and the measured BOLD response is dynamic causal modeling (DCM) (Friston et al., 2003; Marreiros et al., 2008; Stephan et al., 2007, 2008). DCM employs a generative or forward model developed specifically to enable statistical inference about effective connectivity (defined as the influence one brain area exerts over another (Friston, 1994)) between brain areas from indirect BOLD

E-mail addresses: m.havlicek@maastrichtuniversity.nl (M. Havlicek), kamil.uludag@maastrichtuniversity.nl (K. Uludag).
[1] Department of Cognitive Neuroscience, Maastricht Brain Imaging Centre (MBIC), Faculty of Psychology & Neuroscience, Maastricht University, PO Box 616, 6200MD Maastricht, The Netherlands.
[2] Visiting address: Oxfordlaan 55, 6229ER, The Netherlands.
[3] Fax: +31 43 3884125.

[4] Note that the fMRI signal as measured with standard GRE MRI sequence is also directly dependent on CBV in addition to the BOLD effect (Uludağ et al., 2009). Nevertheless, in the following, we will continue to use both terms (i.e. fMRI and BOLD signal) synonymously in accordance with current nomenclature.

http://dx.doi.org/10.1016/j.neuroimage.2015.07.078

measurements. The inversion of this model using a Bayesian inference approach allows one to determine local neuronal and vascular parameters in addition to connectivity parameters among brain areas (Friston et al., 2003, 2007).

Standard DCM for fMRI (which we will refer to as S-DCM here) is based on an approximation of neuronal dynamics with one excitatory state per brain region-of-interest (Friston et al., 2003; Stephan et al., 2007). The neurovascular coupling (NVC), linking neuronal activity and CBF, was designed to include negative feedback between the blood flow level and neuromediators inducing blood flow changes (Friston et al., 2000). The blood flow signal then causes a blood volume and oxygenation response as described by the balloon model (Buxton et al., 1998b), albeit under the assumption of steady-state coupling between flow and volume. Marreiros et al. (2008) extended the standard DCM by entertaining a two-state neuronal model comprising excitatory and inhibitory neuronal populations in each area or node (termed 2S-DCM in the following). Stephan et al. (2008) further allowed for nonlinear interactions between the neuronal states of different areas. A revision of the nonlinear BOLD equation (Stephan et al., 2007) considered a re-parameterization based on coefficients derived by Obata et al. (2004). In this form, with or without the aforementioned extensions of the neuronal model, DCM has been used for the analysis of fMRI data for more than a decade.[5]

In this paper, we discuss some limitations of the generative models utilized in current DCMs and motivate model extensions that are inspired by several robust experimental observations in animal electrophysiology and human/animal fMRI, namely:

1. Both local field potentials (LFPs) and multi-unit activity (MUA) neuronal responses to sustained stimuli typically have an initial peak (overshoot) followed by a decay to a lower steady-state plateau level during stimulation and a deactivation dip ('neuronal post-stimulus deactivation') after the end of stimulus (Hyder et al., 2010; Logothetis, 2002; Logothetis and Wandell, 2004; Shmuel et al., 2006).
2. A change in the neuronal activity starts a cascade of biochemical processes, comprising many neurovascular agents (for recent overview see Riera and Sumiyoshi (2010)) that transform neuronal activity to CBF changes in a predominantly feedforward direction (Attwell et al., 2010; Attwell and Iadecola, 2002; Cauli and Hamel, 2010; Uludağ et al., 2004). Importantly, these neurovascular agents are known to be active during the entire period of neuronal activation (Gordon et al., 2008; Lecrux et al., 2011; Takano et al., 2006; Zonta et al., 2003); i.e., if the level of neuronal activation is altered, the level of vasoactive signal changes as well. This indicates a close relationship between the neuronal activity and CBF changes (in the healthy brain).
3. A CBF post-stimulus undershoot, if present at all, is usually weaker than the BOLD post-stimulus undershoot. There are cases where a post-stimulus undershoot is observed in both CBF and BOLD responses (Mayhew et al., 2014; Sadaghiani et al., 2009), but also cases where it is only present in the BOLD response (Obata et al., 2004).
4. Several studies report a slow return of venous CBV to baseline, comparable in duration to the BOLD post-stimulus undershoot, which persists despite a more rapid return of CBF to baseline (Chen and Pike, 2009; Huber et al., 2014; Kim and Ogawa, 2012; Mandeville et al., 1998).
5. A post-stimulus BOLD undershoot is a commonly but not always observed feature of the BOLD response that may last twice as long as the stimulus duration (Frahm et al., 1996; Krüger et al., 1996). It is known that the duration and magnitude of the post-stimulus BOLD undershoot is dependent on the stimulus type and duration (Bandettini et al., 1997; Hoge et al., 1999; Sadaghiani et al., 2009).
6. In many fMRI data-sets obtained using sustained stimuli, an initial overshoot is observed before the CBF or BOLD signal settles down to a new steady-state value. This adaptive profile of both CBF and BOLD responses is dependent on the type of stimulus and is usually thought to be associated with the neuronal overshoot (see above) (Boynton et al., 1996; Hoge et al., 1999; Sadaghiani et al., 2009). Both the overshoot and the post-stimulus undershoot in the BOLD signal are now believed to reflect different neuronal information (Krekelberg et al., 2006; Mullinger et al., 2013; Sadaghiani et al., 2009) in addition to the vascular contributions — and may thus provide an extra window on brain processes and physiology in both healthy and diseased subjects.

In summary, the observed BOLD dynamics reflect both neuronal and – potentially uncoupled – vascular dynamics. It is the aim of any generative model of the BOLD signal to accurately model the neuronal activity and to effectively disentangle the neuronal and vascular parameters.

In the following, we describe the current DCM generative models and compare them with a new family of DCMs motivated by aforementioned physiological observations (P-DCM). The proposed extensions in P-DCM concern: i) an adaptive two-state neuronal model that accounts for a wide range of neuronal time courses during stimulation and post-stimulus deactivation; ii) a NVC model that links neuronal activity to blood flow in a strictly feedforward fashion; and iii) a balloon model that can account for a vascular uncoupling between blood flow and blood volume due to viscoelastic properties of venous blood vessels.

Theory: from neuronal activity to the BOLD signal

Dynamic causal modeling

DCM assumes model of distributed neuronal activity — and relates this activity to measurable quantities. This generative model entails two types of causal relationships: one between (but also within) neuronal regions representing distributed neuronal interactions (the neuronal model), while the other is a physiological and physical transformation of the neuronal to the measured signal (the biophysical transformation model).

In the case of fMRI data, DCM relies on four basic components that together create the complete forward model: (1) neuronal activity; (2) neurovascular coupling; (3) hemodynamic states; and (4) the BOLD signal (Fig. 1). As the generative models within the DCMs can also be applied to model a single ROI, we will first start with models of a single hemodynamic region (or node) and then consider the effective connectivity among regions.

Neuronal models

Single-state (S-DCM)

In S-DCM (Friston et al., 2003), the neuronal activity is modeled using a single-state that summarizes the synaptic activity in a cortical region of a single (excitatory) neuronal population:

$$\frac{dx_E(t)}{dt} = -\sigma \cdot x_E(t) + c \cdot u(t). \tag{1}$$

This differential equation models temporal changes in the neuronal state $x_E(t)$ that are driven by exogenous input $u(t)$ (e.g. sensory stimuli). The strength of the input influence, which is proportional to the amplitude change of the neuronal signal, is encoded by the parameter c. The temporal scaling of neuronal responses to the exogenous input is controlled by the intrinsic decay parameter σ (i.e. self-connection). In particular, σ controls the rate of exponential growth/decay of the neuronal activity during and after stimulation. This parameter is enforced to be

[5] In this work, we do not consider other DCM versions and extensions such as stochastic DCM (Li et al., 2011).
nonlinear DCM (Stephan et al., 2008) or spectral DCM (Friston et al., 2014), as they all use the same physiological forward model as either S-DCM or 2S-DCM. In other words, any changes in the physiological forward model proposed here are also applicable to these extensions.

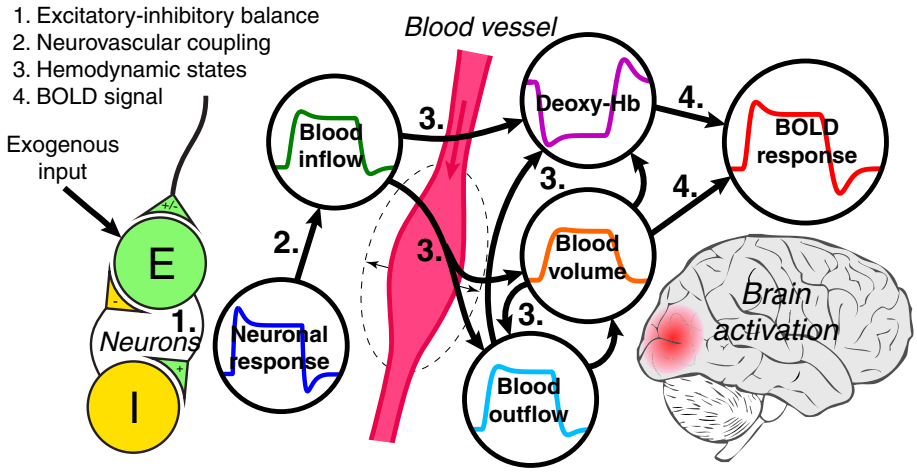

Fig. 1. A schematic illustration of the causal chain between the neuronal and the BOLD response that underlies P-DCM. The neuronal model (1) reflects the excitatory–inhibitory balance, which evokes hemodynamic changes via feedforward neurovascular coupling (2) and causes changes in blood inflow. Changes in blood inflow are accompanied by changes in blood outflow, blood volume and deoxyhemoglobin content (3). The rate of blood outflow is influenced by the change in the blood volume. Changes in blood volume and deoxyhemoglobin content are then reflected in the BOLD response (4).

negative to ensure that the dynamic system is stable, i.e. neuronal signal will return to the baseline after the end of the stimulus.[6]

Two-state (2S-DCM)

The single-state neuronal model was extended by Marreiros et al. (2008) by adding an inhibitory neuronal subpopulation within each region. That is, it models both excitatory (glutamatergic) and inhibitory (GABAergic) connections within each cortical region — making it more realistic from the physiological point of view. This model is represented by a system of two coupled linear differential equations:

$$\begin{aligned}\frac{dx_E(t)}{dt} &= -\sigma \cdot x_E(t) - \mu \cdot x_I(t) + c \cdot u(t),\\ \frac{dx_I(t)}{dt} &= x_E(t) - x_I(t).\end{aligned} \tag{2}$$

The first equation summarizes the dynamics of excitatory neurons $x_E(t)$, while the latter models the activity of inhibitory neurons $x_I(t)$. As before, the excitatory self-connection σ is constrained to be negative, but in contrast to the single-state, it is fixed to 0.5 (in SPM12). The inhibitory self-connection is also fixed to the value of − 1. This negativity constraint ensures stability (i.e., the real parts of the eigenvalues of the system's Jacobian are negative); in other words, the neuronal dynamics eventually collapse to a stable steady-state. In addition, the excitatory–inhibitory connection is also fixed to the value of 1. The effect of neuronal inhibition is introduced by negative feedback between the inhibitory and excitatory state, which is scaled by the parameter μ with a default prior value of $\mu = 1/8$. The negative inhibitory–excitatory connection in combination with the positive excitatory–inhibitory connection results in complex eigenvalues, which determine the oscillatory frequency of this dynamic system; it is about 0.04 Hz for the default setting.

Adaptive two-state (P-DCM)

To overcome the limitations of the two-state model (see Results section), we introduce a new two-state neuronal model, which allows for more flexible and adaptive neuronal responses — similar to observed physiological recordings (for example, as obtained from invasive and non-invasive electrophysiology). The new neuronal model can be partly related to the model used in Buxton et al. (2004), which was defined as a discrete model with continuous component model neuronal inhibition. Here we consider continuous models for both excitatory and inhibitory states:

$$\begin{aligned}\frac{dx_E(t)}{dt} &= -\sigma \cdot x_E(t) - \mu \cdot x_I(t) + c \cdot u(t),\\ \frac{dx_I(t)}{dt} &= \lambda \cdot (x_E(t) - x_I(t)).\end{aligned} \tag{3}$$

The dynamics of the excitatory neuronal state are described by the same equation as above. In contrast to 2S-DCM and S-DCM, the excitatory self-connection σ is free but not region-specific. This assumption is consistent with an early version of DCM for fMRI (Friston et al., 2003). The dynamics of the inhibitory state are driven by the excitatory state and scaled with inhibitory gain factor λ. This gain factor allows controlling both the relative amplitude of the inhibitory activity with respect to the excitatory activity and its temporal smoothness. Differences in temporal smoothness between excitatory and inhibitory activity result in temporary imbalance that can cause adaptation of the neuronal response. How much this temporary imbalance is reflected in the excitatory activity is controlled by the inhibitory–excitatory connection μ. As such, the overall dynamic interaction (or balance) between excitatory and inhibitory activity is controlled by both the inhibitory gain factor λ and the inhibitory–excitatory connection μ (see Table 1A for their values). This means, that these parameters introduce adaptation and

Table 1A
Recommended parameter values for P-DCM and their plausible ranges (in brackets).

Parameter	Name	Value
Intrinsic neuronal connectivity		
σ (Hz)	Excitatory self-connection	0.5 (0.1–1.5)
μ (Hz)	Inhibitory–excitatory connection	0.4 (0–1.5)
λ (Hz)	Inhibitory gain factor	0.2 (0–0.3)
Neurovascular coupling		
φ (Hz)	Decay of vasoactive signal	0.6
ϕ (Hz)	Gain of vasoactive signal	1.5
χ (Hz)	Decay of blood inflow signal	0.6
Hemodynamic model		
t_{MTT} (sec)	Mean transit time	2 (1–5)
τ (sec)	Viscoelastic time	4 (0–30)
α	Grubb's exponent	0.32
E_0	Oxygen extraction fraction at rest	0.4
Physical BOLD signal model (Part I)		
V_0 (%)	Venous blood volume fraction	4

[6] Usually, positivity or negativity of connections is imposed using log-normal priors, i.e. the parameters from normal distributions are transformed via an exponential function, which is multiplied by a scaling parameter that defines the mean of log-normal distribution (see also Supplementary Material S5). For example, for negative constraints, we have $-\sigma \exp(\bar{\sigma})$, and the variable $\bar{\sigma}$ is sampled from the normal distribution.

refractory effects to neuronal response; i.e. how fast the activity of excitatory neuronal response drops from its initial peak to the plateau level and how fast it returns from the post-stimulus dip to the baseline. Additionally, strengths of μ and λ connections are relative to the strength of σ, which determines the overall temporal scaling of the neuronal dynamics. For example, a decrease of σ will lead to a decrease in λ and μ (see Supplementary Material S1 for more detailed analysis of this multi-dimensional parameter space). Finally, it is also worth noting that the new two-state model can be reduced to the old two-state model by setting $\lambda = 1$ or to the single-state model by setting $\mu = 0$.

Neurovascular coupling

Neurovascular coupling links changes in neuronal activity to changes in CBF and CBV. There are many neurovascular agents that are involved in transforming neuronal activity to hemodynamic changes (Riera and Sumiyoshi, 2010). It is beyond the scope of the current article to discuss those. Please see specialized reviews on that topic; e.g. (Attwell et al., 2010; Cauli et al., 2004; Devor et al., 2007; Lauritzen, 2005; Riera and Sumiyoshi, 2010).

S-DCM and 2S-DCM differ only in their neuronal model (and the ensuing connectivity model). Both are identical in NVC, vascular dynamics and the observation model.

Feedback based neurovascular coupling (S-DCM and 2S-DCM)

Based on the empirical evidence that the relationship between neuronal activity and blood flow is roughly linear (Miller et al., 2001), Friston et al. (2000) introduced an NVC model assuming a linear drive between neuronal activity and blood flow change. In this model, the neural activity creates an inducing signal $s(t)$ that drives blood flow $f(t)$ in a linear way, with $f(t)$ responding like a damped harmonic oscillator. That is, the flow changes are evoked by the inducing signal (feedforward) and the level of flow in turn changes the inducing signal (feedback):

$$\begin{aligned}\frac{ds(t)}{dt} &= -\kappa \cdot s(t) - \gamma \cdot (f(t) - 1) + x_E(t),\\ \frac{df(t)}{dt} &= s(t).\end{aligned} \tag{4}$$

Regulated by rate constants γ and κ, it produces damped oscillations with a frequency about 0.09 Hz (consistent with ultra-slow endogenous fluctuations in BOLD signals (Biswal et al., 1995; Fox et al., 2005; Fransson, 2005) and empirical observations of the vasomotor or V-signal; see Discussion). This mathematical formulation implies that the blood flow exhibits a post-stimulus undershoot even with no neuronal post-stimulus deactivation. At first glance, this form seems suitable for short stimuli, where the increase of neuronal activity leads to increase of the inducing signal, which in turn results in an increase of CBF. However, for sustained stimulation, the neuronal activity settles to the steady-state plateau (and so does CBF), while the inducing signal $s(t)$ is altered only at the beginning and the end of stimulation. Additionally, any manipulation of the CBF baseline with no neuronal activity change (e.g. using vasodilatory agents) leads to opposite changes in $s(t)$, which is physiologically implausible (see Supplementary Material S2 for more details). Furthermore, the formulation of feedback based NVC (4) should not be confused with the hypothesis that CBF is locally controlled by the level of tissue concentrations of oxygen and glucose determined by baseline CBF, metabolism and neuronal activity (see review by Attwell et al. (2010) and Supplementary Material S2).

Several studies which manipulated blood O_2 (Lindauer et al., 2010) and glucose (Powers et al., 1996) concentrations have shown that O_2 and glucose do not regulate blood flow according to the negative-feedback hypothesis (Attwell et al., 2010). It is currently believed that neurovascular coupling is regulated by predominantly feedforward mechanisms (within the range of stimulus evoked responses in healthy human subjects). This means that neurons either signal directly to blood vessels via synapses or extra-cellular diffusion or activate astrocytes to release vasoactive agents onto the vessels (Attwell and Iadecola, 2002; Cauli et al., 2004; Devor et al., 2007; Lauritzen, 2005; Masamoto and Kanno, 2012; Uludağ et al., 2004; Zonta et al., 2003). Additional evidence for the feedforward mechanism is provided by hypercapnia experiments, which show that increasing baseline CBF only minimally affects stimulus-induced CBF change (Brown et al., 2003; Li et al., 2000; Zappe et al., 2008b): The negative feedback hypothesis predicts a much smaller stimulus-induced CBF change with higher baseline CBF values.

Feedforward neurovascular coupling (P-DCM)

Following these arguments, therefore, we consider an NVC model for P-DCM based strictly on feedforward mechanisms. Thus, we have chosen (under the constraint that the dynamical system linking synaptic activity and blood flow is linear) the most parsimonious model that represents these mechanisms:

$$\begin{aligned}\frac{da(t)}{dt} &= -\varphi \cdot a(t) + x_E(t),\\ \frac{df(t)}{dt} &= \phi \cdot a(t) - \chi \cdot (f(t) - 1).\end{aligned} \tag{5}$$

Here, $a(t)$ is a vasoactive signal that transforms the neuronal response $x_E(t)$ to the blood flow response $f(t)$. Although the NVC is modeled to be driven only by excitatory neuronal activity, the contribution of inhibitory activity to it is introduced indirectly through interactions between the two neuronal populations. Eq. (5) represents a simple (dynamic) convolution kernel, which acts as a positively constrained low-pass filter of the neuronal dynamics. This is achieved using three regulatory constants φ, ϕ and χ which control the response decay and can delay its peak by about 3–5 s with respect to the neuronal signal, as observed experimentally. Parameterization of this NVC was adjusted to approximate the gamma convolution kernel previously used to link the neuronal response to blood flow (Buxton et al., 2004). These regulatory constants are fixed in this paper to produce about 3 s delay of the CBF response peak, with respect to a short input impulse (for specific values see Table 1A). However, if CBF measurements are available together with the BOLD signal, then χ can be optimized as a free parameter.

The basic physiological interpretation of this model is that the neuronal activity starts a cascade of biochemical processes that – for neuronal excitation/inhibition – leads to arterial vasodilatation/vasoconstriction associated with increased/decreased CBF (Devor et al., 2007). Effectively, this means that the vasoactive signal and blood flow are accurate representations of low-pass-filtered neuronal responses. As a consequence, in contrast to the feedback based NVC used in S-and 2S-DCM, an observed CBF post-stimulus undershoot is always related to neuronal deactivation (Masamoto et al., 2008).

Hemodynamic model

The hemodynamic model used in DCM was motivated by the balloon model (Buxton et al., 1998b). This model assumes that post-capillary vessels are represented by an expandable venous compartment (i.e. a balloon) that is fed by the output of the capillary bed, $f(t)$; i.e. by the output of the NVC. The coupled equations of the original balloon model represent mass balance for blood volume and deoxyhemoglobin as they pass through the venous balloon[7]:

$$\frac{dv(t)}{dt} = \frac{1}{t_{MTT}}\left[f(t) - f_{out}(v,t)\right], \tag{6}$$

[7] Note that the CBV and deoxyhemoglobin in the balloon model refer almost exclusively to changes in the venous part of tissue vasculature. However, the total CBV (Huber et al., 2014; Kim and Ogawa, 2012), which is usually the variable determined in experiments, represents a weighted sum of arterial, capillary and venous CBV that is not directly considered in the balloon model. In general, the arterial, capillary and venous CBV are causally linked. While the changes in arterial and capillary CBV follow closely the dynamic change in CBF, the change in venous CBV can be more delayed with respect to CBF (see below the CBF–CBV uncoupling).

$$\frac{dq(t)}{dt} = \frac{1}{t_{MTT}}\left[f(t)\frac{E(f)}{E_0} - f_{out}(v,t)\frac{q(t)}{v(t)}\right]. \quad (7)$$

The two dynamical variables are the blood volume $v(t)$ and deoxyhemoglobin content $q(t)$ within the venous balloon, normalized to their values at rest. Here, the rate of change of the blood volume $v(t)$ is modeled as a difference between the blood inflow $f(t)$ and the blood outflow $f_{out}(v)$. The rate of change of deoxyhemoglobin $q(t)$ is modeled as a difference between the rate of delivery of deoxyhemoglobin into the venous balloon and the clearance rate of deoxyhemoglobin from the tissue. The time dimension of these equations is scaled by the time constant t_{MTT}; i.e., the mean transit time that blood takes to pass the veins.

This biomechanical model is based on two functions: oxygen extraction fraction, $E(f)$, and blood outflow, $f_{out}(v)$. Based on the physiological notion of limited oxygen delivery (Buxton and Frank, 1997), a large increase of blood inflow is required to support a small increase in oxygen metabolism ($CMRO_2$). In addition, studies with suppressed hemodynamic response have shown that oxygen extraction from the blood is as slow as the typical hemodynamic response (Masamoto et al., 2008; Zappe et al., 2008a). Thus, these studies suggest a tight temporal coupling between $CMRO_2$ and CBF, albeit with a mismatch in their respective amplitudes (see Discussion section for elaboration and limitation of this concept). Therefore, we model $E(f)$ in S-, 2S- and P-DCM to be a fixed nonlinear function of blood inflow (Buxton and Frank, 1997):

$$E(f) = 1-(1-E_0)^{1/f}, \quad (8)$$

where E_0 is the net oxygen extraction at rest. Normalized $CMRO_2$ is then simply expressed as $f \cdot E(f)/E_0$, which is implicit in Eq. (7). The relationship between blood outflow and blood volume can also differ between the steady-state and transient periods.

Balloon model — steady-state (S-DCM, 2S-DCM)

Steady-state models are concerned primarily with magnitude changes. Grubb et al. (1974) found that the steady-state relationship between CBF and CBV could be described by a power law, so that during steady-state the outflow follows a simple nonlinear relation:

$$f_{out}(v) = v^{1/\alpha}, \quad (9)$$

where α was empirically found to be about 0.38 (Grubb et al., 1974). In other words, CBV change is a (slightly non-linear) scaled version of CBF change. Although this relationship is valid for steady-state conditions, it does not hold during transient responses. Nevertheless, S-DCM and 2S-DCM assume that the steady-state flow-volume relationship (using the value of $\alpha = 0.32$) is also valid during the transient responses.

Balloon model — viscoelastic effect (P-DCM)

Mandeville et al. (1998) experimentally demonstrated that the above Grubb relationship between blood volume and blood outflow holds during the plateau of the positive response but not during the BOLD undershoot period; i.e., there is a different transient relation $f_{out}(v,t)$ in the transition periods between the steady-states. This key observation was crucial for the development of the balloon model, since it allows for the possibility that the post-stimulus BOLD undershoot is primarily a passive biomechanical effect of the blood vessels rather than a metabolic effect (Buxton, 2012). This can be modeled by adding a dynamic viscoelastic effect to the steady-state blood outflow equation (Buxton et al., 1998a, 2004):

$$\begin{aligned} f_{out}(v,t) &= v^{1/\alpha} + \tau \cdot \frac{dv(t)}{dt} \\ &= \frac{1}{\tau + t_{MTT}} \cdot \left(t_{MTT} \cdot v(t)^{1/\alpha} + \tau \cdot f(t)\right). \end{aligned} \quad (10)$$

With this form, the balloon initially resists a change in blood volume, but eventually settles into a new steady-state that conforms to the power law model in Eq. (9). The viscoelastic time constant τ controls the duration of this transient adjustment. For a nonzero value of τ, the outflow follows a different curve during balloon inflation and deflation, contributing to BOLD response overshoot and undershoot, respectively. In P-DCM, we include the viscoelastic effect and follow the original balloon model; i.e., allow for temporal uncoupling of CBF and venous CBV.

Therefore, we propose in P-DCM that the BOLD post-stimulus undershoot (but also response overshoot) can reflect contributions from both: (i) neuronal post-stimulus deactivation carried through the blood flow and (ii) a vascular uncoupling due to a slow recovery of the venous CBV.

Physical BOLD signal model

To connect the above hemodynamic model with experimental fMRI data acquired with the BOLD contrast, Buxton et al. (1998b) introduced a quantitative model of the BOLD signal change as a function of blood susceptibility and volume:

$$y = V_0\left[k_1(1-q) + k_2\left(1-\frac{q}{v}\right) + k_3(1-v)\right]. \quad (11)$$

Here, the first term describes the extravascular signal as pure function of deoxyhemoglobin; the second term describes the intravascular signal given by the ratio between deoxyhemoglobin and blood volume; and the third term describes the volume-weighted balance between extravascular and intravascular signals. V_0 is the resting blood volume fraction and the parameters k_1, k_2 and k_3 are dimensionless constants reflecting baseline physiological properties of brain tissue and acquisition parameters of the gradient echo (GE) sequence. Although V_0 varies over the brain, its actual value is usually not relevant for the DCM formulation because the value of V_0 is just a scaling factor of the BOLD signal, which can be compensated by the scaling constant of neuronal activity. The k_1, k_2 and k_3 parameters are dependent on the magnetic field strength:

$$\begin{aligned} k_1 &= 4.3\vartheta_0 \cdot E_0 \cdot TE, \\ k_2 &= \varepsilon \cdot r_0 \cdot E_0 \cdot TE, \\ k_3 &= 1-\varepsilon. \end{aligned} \quad (12)$$

The term ε denotes the ratio of intra- to extra-vascular fMRI signal contributions. Its exact value, however, has been somewhat controversial in the literature for fMRI data obtained with GE sequences at 1.5 T (see the discussion in Stephan et al. (2007)). Previous studies have assumed values of ε in the range 0.4–1.43. Due to this ambiguity, ε is treated as a free parameter in standard DCMs. The term ϑ_0 is the (field-dependent) frequency offset at the surface of a blood vessel for fully deoxygenated blood and has a value of 40.3 s^{-1} at 1.5 T. Finally, r_0 is the sensitivity (i.e. regression slope) of changes in intra-vascular signal relaxation rate with changes in oxygen saturation, which is fixed to $r_0 = 25$ s^{-1} in standard DCMs based on estimates for 1.5 T (Buxton et al., 1998b; Obata et al., 2004). *TE* is the echo time (in ms).

The above coefficients of the fMRI-BOLD signal equation have not systematically been derived for GE or for spin-echo (SE) MRI acquisition methods at field strengths >3 T. The recent results by Uludağ et al. (2009), however, allow one to determine these parameters for different field strength and acquisition methods. They also suggest revised values for these parameters at 1.5 T and 3 T with GE (see Table 1B): The term ϑ_0 is simply (linearly) proportional to magnetic field strength. The ε values for macro- and micro-vasculature are taken from Fig. 3c for SE and 5c for GE in Uludağ et al. (2009). As can be seen, ε becomes smaller with field strength for both SE and GE, and ε is larger for SE than for GE. For GE, the intra-vascular signal becomes negligible for field strength ≥7 T, which leads to a linearization of BOLD signal equation. Moreover, the measured BOLD signal is expected to have ε more on macro-vascular

Table 1B
Field strength dependence of the BOLD signal parameters.

Physical BOLD signal model (Part II)					
Field strength (T)	ϑ_0	ε for GE (macro–micro)	r_0 for GE	ε for SE (macro–micro)	r_0 for SE /1000
1.5	40.3	0.1263–1.3210	15	14.9693–60	0.0171
3	80.6	0.1291–0.5648	108	1.92–5.4598	0.0684
4	107.5	0.0295–0.1263	157	1.0668–2.7567	0.1216
4.7	126.3	0.0103–0.0463	191	0.7857–1.6963	0.1679
7	188.1	0	–	0.3390–0.3967	0.3725
9.4	252.5	0	–	0.0640–0.2602	0.6717
11.7	314.3	0	–	0.0133–0.1970	1.0406
14.1	378.8	0	–	0.0029–0.1573	1.4900
16.4	440.6	0	–	0.0006–0.1280	2.0446

than micro-vascular side. The term r_0 for SE and GE can be derived from linearizing Eqs. (8) and (9) in Uludağ et al. (2009). Finally, the optimal TE values are also subject to variation with different field strengths and their specific values are given by the acquisition (user-specific) protocol. Therefore, they are not included in the Table 1B (see also Supplementary Material S4 for further demonstration).

Theory: effective connectivity of brain areas

In the previous section, we have focused on a single region — modeling the link between neuronal and hemodynamic responses and the fMRI signal. However, DCM is usually used to study effective connectivity among different brain areas. In fMRI, connectivity patterns can be distorted by the sluggishness of the hemodynamic response and by hemodynamic variability (Roebroeck et al., 2011) in different areas and even nearby voxels. DCM tries to disentangle the neuronal connectivity from these hemodynamic confounds. In the following, we will discuss the inter-area connectivity models in the three different DCMs.

Single-state connectivity model (S-DCM)

The original neuronal model, assuming only an excitatory neuronal population, has a simple form that allows for bilinear interactions between neuronal states and experimentally controlled (and therefore known) inputs. Although we restrict our description only to the standard bilinear form, all neuronal connectivity models (including the ones below) can be extended to also include nonlinear interactions as described by Stephan et al. (2008). The bilinear model is represented by a multiple-input multiple-output system that is described by a set of differential equations written in matrix form as:

$$\frac{dX_E(t)}{dt} = \Im X_E(t) + CU_d(t),$$
where
$$\Im_{ij} = A_{ij} + \Sigma_{m=1}^{M} B_{ij}^{(m)} u_m(t),\ for\ i \neq j,\ and$$
$$\Im_{ii} = -\sigma \exp\left(A_{ii} + \Sigma_{m=1}^{M} B_{ii}^{(m)} u_m(t)\right). \quad (13)$$

This differential equation models temporal changes in a multivariate neuronal state $X_E(t) = [x_{E1}(t), \ldots, x_{EN}(t)]^T$, where 1, …, N indexes regions-of-interest (ROIs), resulting from a sum of three effects. First, the off-diagonal element matrix of A_{ij} encodes the fixed (context independent) strength of connections between brain regions, whereas the diagonal elements of A_{ii} scale the self-connection σ that was described above to ensure stability and decay of neuronal responses.[8] Second, the matrix $B^{(m)}$ represents the context-dependent modulations of connections induced by (modulatory) exogenous inputs $u_m(t)$. Above, we chose to group these A and B matrices into the total connectivity matrix $\Im$ to simplify the notation. Third, the matrix C encodes the influence of the (driving) exogenous inputs $U_d(t) = [u_{d1}(t), \ldots, u_{dN}(t)]^T$ to the system.

The strength of connections (in units of Hz) among regions is relative to the excitatory self-connections. This means that we deal with normalized parameters. They can have either positive or negative values; i.e., they generate either positive or negative neuronal responses at the terminal node of the feedforward connection, or they positively or negatively modulate the neuronal response via feedback connections. Finally, the usual interpretation of positive connections is that they represent neuronal excitation, whereas negative connections represent neuronal inhibition.

Two-state connectivity model (2S-DCM)

The standard two-state neuronal model (Marreiros et al., 2008), which added an inhibitory neuronal subpopulation to the excitatory neuronal subpopulation within each region, has the following multivariate form to model bilinear neuronal interactions between different brain regions:

$$\frac{dX_E(t)}{dt} = \Im^{+} X_E(t) + \Im^{-} X_I(t) + CU_d(t),$$
$$\frac{dX_I(t)}{dt} = X_E(t) - X_I(t),$$
where
$$\Im_{ij}^{+} = \exp\left(A_{ij} + \Sigma_{m=1}^{M} B_{ij}^{(m)} u_m(t)\right)/8, \Im_{ij}^{-} = 0, \} \text{for},\ i \neq j \text{and}$$
$$\Im_{ii}^{+} = -\sigma I,$$
$$\Im_{ii}^{-} = -\exp\left(A_{ii} + \Sigma_{m=1}^{M} B_{ii}^{(m)} u_m(t)\right)/8. \quad (14)$$

The long-range extrinsic connections are modeled as excitatory. This is in accordance with known anatomy: the vast majority of long-range connections are mediated by excitatory neurons (Markram et al., 2004). The main differences with respect to the single-state neuronal model are twofold: First, although the extrinsic connections are assumed to be excitatory, the activity of the excitatory neuronal state also carries an indirect contribution of the inhibitory state due to the dynamic local interactions between the two neuronal populations. Second, the activity is propagated to other regions though the connectivity matrix $\Im_{ij}^{+}$ and its off-diagonal elements (i.e. extrinsic connections) are constrained to positive values (highlighted by + superscript), which means that this model lacks a neuronal mechanism to express inhibitory effects of one area over another or simply to explain neuronal deactivation (see below).

The model allows for region specific modulation of inhibitory to excitatory connections, encoded in the diagonal matrix elements $\Im_{ii}^{-}$, by context dependent inputs. Notice that for zero diagonal elements A_{ii} with the absence of additive modulatory diagonal elements $B_{ii}^{(m)}$, $\Im_{ii}^{-}$ is equivalent to above inhibitory–excitatory connection with default value $-\mu = -1/8$. Next, the excitatory self-connections on the diagonal of matrix $\Im_{ii}^{+}$ (i.e. σI, where I is identity matrix) have fixed values in newer implementations (e.g. SPM12 code R5672). This means that they are neither region-specific nor can be modulated by context-dependent input.

Adaptive two-state connectivity model (P-DCM)

In developing the new adaptive two-state neuronal connectivity model, we wanted to overcome the limitations of the standard DCM models described above, to more accurately explain neuronal responses commonly observed in both direct electrophysiological recordings and

[8] Note that the scaling of σ via log-normal transformation was introduced in later versions (the SPM12 implementation). In earlier implementations, σ was directly expressed by diagonal elements of A and B — σ remains negative.

indirect fMRI measurements. To this end, we consider the following multivariate form of the new two-state model:

$$\begin{aligned}
&\frac{dX_E(t)}{dt} = \Im X_E(t) + \Im^{-} X_I(t) + CU_d(t),\\
&\frac{dX_I(t)}{dt} = \mathfrak{G}(X_E(t) - X_I(t)),\\
&\text{where}\\
&\left.\begin{aligned}
\Im_{ij} &= A_{ij} + \Sigma_{m=1}^{M} B_{ij}^{(m)} u_m(t),\\
\Im_{ij}^{-} &= 0,\\
\mathfrak{G}_{ij} &= 0,
\end{aligned}\right\} \text{ for } i \neq j, \text{ and}\\
&\Im_{ii} = -\sigma \exp\left(\tilde{\sigma} + \Sigma_{m=1}^{M} B_{ii}^{(m)} u_m(t)\right),\\
&\Im_{ii}^{-} = -\mu \exp\left(\tilde{\mu}_i + \Sigma_{k=1}^{K} b_{\mu i}^{(k)} u_{\mu k}(t)\right),\\
&\mathfrak{G}_{ii} = \lambda \exp\left(\tilde{\lambda}_i + \Sigma_{l=1}^{L} b_{\lambda i}^{(l)} u_{\lambda l}(t)\right).
\end{aligned} \tag{15}$$

As in 2S-DCM, the long-range connections in matrix $\Im_{ij}$ are modeled between the excitatory neuronal populations. However, these connections can be both positive and negative, which lead to either increase or reduction of neuronal activity in the target area, respectively. Then, the total connectivity matrix $\Im$ thus has a very similar form as in the original single-state model (Friston et al., 2003), including the additive modulatory effects encoded in matrix $B^{(m)}$ and controlled by the modulatory inputs $u_m(t)$. Clearly, this is a simplification with respect to the long-range neuronal connections; however, the complexity of the neuronal model must be tailored to the amount of information present in the experimental fMRI data. Moreover, to make this neuronal model generalizable to broad variations in experimental conditions and observations, we allow also the local connections – responsible for controlling the balance between excitatory and inhibitory neurons – to be modulated by context dependent inputs $u_{\mu k}(t)$ and $u_{\lambda l}(t)$. These inputs scaled by parameters $b_{\mu i}^{(k)}$ and $b_{\lambda i}^{(l)}$ can modulate the inhibitory-excitatory connections and inhibitory gain factors, respectively. Note that all these parameters can be region-specific. In general, introducing modulation of intrinsic connections can be used to model different neuronal dynamics during sustained stimulation and during post-stimulus intervals. For example, one can imagine that there is a strong adaptation profile during stimulation, followed by minimal or no post-stimulus deactivation (see experimental data below).

Simulations and experimental data

In this section, we describe the simulations to characterize the basic phenomenology of the models, paying special attention to the empirical aspects of neuronal, neurovascular and hemodynamic responses detailed in the Introduction. We first consider the responses of a single region and then the responses of a simple network. Finally, the importance of introducing new physiologically more informed models is demonstrated using an experimental BOLD-fMRI example.

Impulse response functions in a single ROI

To illustrate the variety of time courses within a single region of interest (ROI) that can be produced by S-DCM, 2S-DCM and P-DCM, we describe responses of the dynamic system to a boxcar input function with 1 s (short) and 30 s (long) durations, respectively. These responses were calculated by numerical integration of dynamic systems using local linearization (Ozaki, 1992) in the MATLAB software (MathWorks), with integration step in $\Delta t = 0.01$ sec.

The parameters used to simulate neuronal and hemodynamic responses can be found in Table A.1. These were chosen to give a basic idea of the response variability supported by specific DCMs. Note that the amplitude of the input function that drives the neuronal model was always adjusted to produce ~50% CBF response change, a typical magnitude in human functional stimulation experiments. Finally, all S-, 2S- and P-DCM assumed a parameterization of the BOLD signal equation given for 3 T field strength (see Tables 1A,1B), acquired with a GE sequence and $TE = 35$ ms (simulations with different TE's produce very similar results – data not shown – within a range of 30 to 45 ms).

Connectivity simulations

To examine the basic properties of connectivity models and how they are reflected in the BOLD signals, we generate BOLD responses by assuming a simple neuronal network of three connected regions (Fig. 2A). In this network, the R_1 region is driven by exogenous input (i.e. two repetitions of simple boxcar function of 30 s duration) and the activity from region R_1 is propagated to regions R_2 and R_3. Between R_1 and R_2 regions, we consider a strong positive feedforward connection, which persists during both periods. We also introduce a positive feedback connection through a modulatory input, which is active during the first stimulation period, but also after the first stimulus offset. In contrast, between R_1 and R_3 regions, we consider a negative feedforward connection. Specific values for connections of this network are displayed in Fig. 2A.

First, we simulated all neuronal connectivity models with values of extrinsic and intrinsic excitatory connections reported in Fig. 2A, and then also considered a scenario where these connections were half the size. By doing this, we were able to compare BOLD responses given faster (scenario 1) and slower (scenario 2) neuronal dynamics. This has partially historical reasons; earlier versions of DCMs considered fast neuronal dynamics but later – with the introduction of stochastic DCM (Daunizeau et al., 2009; Friston et al., 2008, 2010; Havlicek et al., 2011) that allowed modeling of endogenous neuronal activity – the self-inhibitory connections in the excitatory state were adjusted to account for slower dynamics. In our connectivity simulations, only the neuronal parameters were varied (see Fig. 2B) and the neurovascular and hemodynamic parameters were kept constant. However, to demonstrate the sole effect of neuronal dynamics on the BOLD responses, the CBF–CBV uncoupling was (artificially) minimized by setting $\tau = 0$. A summary of all parameters used to calculate the neuronal and hemodynamic responses defined by different models can be found in Table A.2. As for the single region simulations, S-, 2S- and P-DCM assumed a parameterization of BOLD signal equation for 3 T field strength, acquired with GE sequence and $TE = 35$ ms.

Evaluation of model evidence using experimental data

We illustrate the relevance of the different physiological mechanisms embedded within the different DCMs on single ROI experimental fMRI responses during a visual task. In short, the visual task involved alternation between static and flickering checkerboards organized in blocks (each 55 s long) and interleaved with resting periods (each 110 s long). The functional data were measured with an ASL sequence at 3 T providing both BOLD and CBF responses. Significantly activated voxels from the left V1 region of visual cortex were selected for the purpose of model comparison. Details about data acquisition, preprocessing and ROI selection can be found in Supplementary Material S5.

For model comparison, we restrict our analysis only to the BOLD responses averaged over all trials of the two conditions. To this end, each model is driven by two inputs representing static and flickering visual stimulation and selected intrinsic neuronal connections were modulated by four unique modulatory inputs. These modulatory inputs are specifically designed to distinguish between stimulus and post-stimulus intervals in each condition (see Fig. 2C for schematic illustration). This means that we allow for different parameterization of neuronal model, between conditions but importantly also between stimulus and post-stimulus intervals. In particular, in S-DCM we modulate the excitatory self-connection (σ); in 2S-DCM the inhibitory–excitatory connection (μ); and in P-DCM the excitatory self-connection (σ) and inhibitory–excitatory connection (μ). The inhibitory gain factor (λ) is estimated as well, but it is (in this case) assumed constant over all

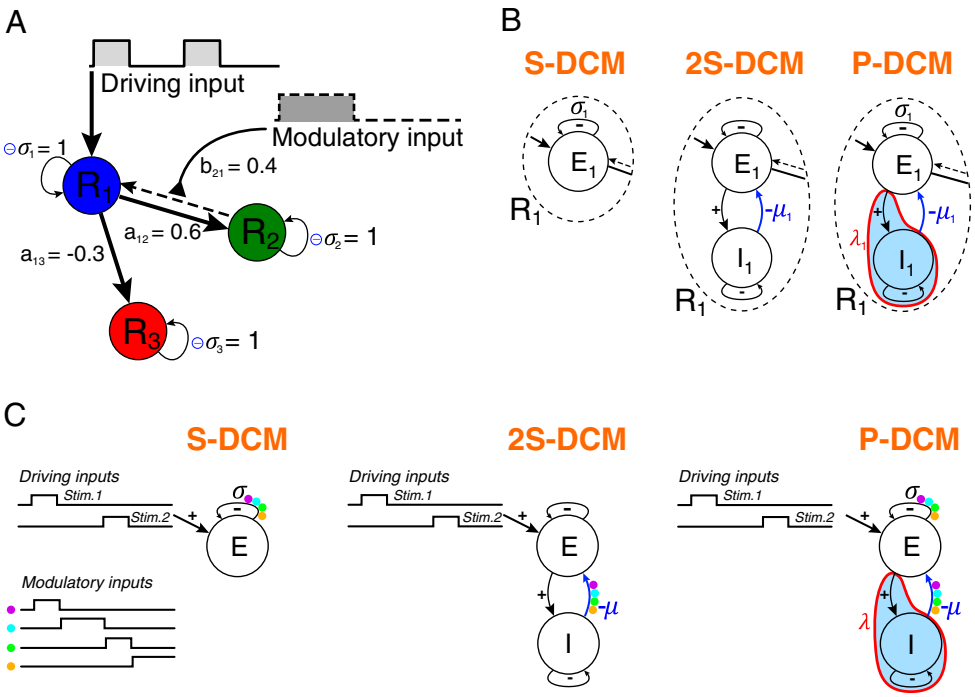

Fig. 2. An exemplary neuronal network used for simulations. (A) Network of three nodes with one driving and one modulatory input. Connection strengths in this network represent the first simulation scenario (see text for details). For the second scenario these values were reduced to half. (B) The intrinsic structures of a single brain area as described by different DCMs. This intrinsic structure was also subject to variation between the two scenarios (besides the extrinsic connections): S-DCM assumed first an excitatory self-connection $\sigma = 1$ Hz and then $\sigma = 0.5$ Hz; 2S-DCM assumed the excitatory self-connection and an inhibitory–excitatory connection $(\sigma, \mu) = (1, 0.25)$ Hz for the first scenario and $(\sigma, \mu) = (0.5, 0.125)$ Hz for the second scenario; P-DCM assumed first $(\sigma, \mu, \lambda) = (1, 0.4, 0.15)$ Hz and then $(\sigma, \mu, \lambda) = (0.5, 0.2, 0.15)$ Hz, where the inhibitory gain factor λ stayed constant for both scenarios. (C) A schematic illustration of the model specification by the means of driving and modulatory inputs for S-DCM (left), 2S-DCM (middle), and P-DCM (right) as assumed within the model inversion.

conditions and time intervals (see Fig. 2C). Further, while S-DCM and 2S-DCM allowed fitting of the decay parameter (κ) in the feedback based NVC, the decay parameter (χ) of the feedforward NVC was fixed. All DCMs allowed fitting the mean transit time (t_{MTT}) and the relative intra to extra-vascular signal contribution (ε). In P-DCM, we additionally enabled fitting of the viscoelastic time (τ). For default values of all new model parameters see Table 1A. Models were inverted using a Variational Bayesian algorithm (Friston et al., 2007) implemented in SPM12 and compared on the basis of the model log-evidence difference (approximated by the difference between Variational free energies of the different models; see Supplementary Material S5).

Results

Impulse response functions in a single ROI

The curves in Figs. 3 and 4 illustrate the variety of time courses that can be produced by S-DCM, 2S-DCM and P-DCM, respectively. In each figure, the time courses of neuronal, CBF, CBV, and BOLD responses are shown in separate panels.

S-DCM

In Fig. 3A, the neuronal response (to a short stimulus) based only on excitatory activity increases during stimulation interval and exhibits decay to the baseline during post-stimulus interval. The CBF response rises more slowly than the neuronal activity and, for different values of the signal decay constant κ, demonstrates post-stimulus CBF undershoots that vary from very strong (~20% compared to the positive peak) to negligible. The CBV response is slightly delayed with respect to CBF response due to the mean transit time of $t_{MTT} = 2$ s. The dynamics of CBV follow the dynamics of the CBF response very closely, including its non-neuronal dynamic transients. Note that the recovery to baseline of the BOLD signal is slower than that of CBF and CBV, in discrepancy with experimental data (see e.g. Sadaghiani et al. (2009), Chen and Pike (2009) or Huber et al. (2014)). In addition, the BOLD signal undershoot is smaller than that of CBF. It is worth noting that t_{MTT} can affect the presence of post-stimulus undershoot as it is observed in the BOLD response: for $t_{MTT} > 3$ s, there is no BOLD post-stimulus undershoot, even though the post-stimulus undershoot would still be present at the level of CBF and CBV (see results from experimental data below).

In Fig. 4A, we show the time courses for the same model parameters but induced by sustained stimulation. Here, the neuronal response first exponentially grows until it reaches (in ~5 s) a steady-state plateau and then it exponentially decays after stimulus cessation. A small initial overshoot and post-stimulus undershoot in the CBF responses are conveyed to the CBV and less to the BOLD responses. Note that varying the feedback parameter in NVC has only a small effect on the resulting BOLD responses.

2S-DCM

In Fig. 3B, the neuronal response to a short impulse stimulation exhibits richer dynamic transients compared to the single-state model. This was achieved by altering the inhibitory–excitatory connection parameter μ. These neuronal responses mainly affect the CBF return to baseline and the CBF response width. However, they only have a negligible influence on the CBF post-stimulus undershoot amplitude. Dynamic transients of CBF responses are conveyed further to CBV and BOLD responses, with the BOLD responses again showing slightly smaller post-stimulus undershoot compared to the CBF responses. Note that even though we have varied the neuronal post-stimulus deactivation from strong (~25% compared to the positive peak) to none, these neuronal variations are not reflected in the post-stimulus BOLD undershoot but only slightly in the BOLD response width. This is because the inhibitory activity is very closely coupled to the excitatory activity and

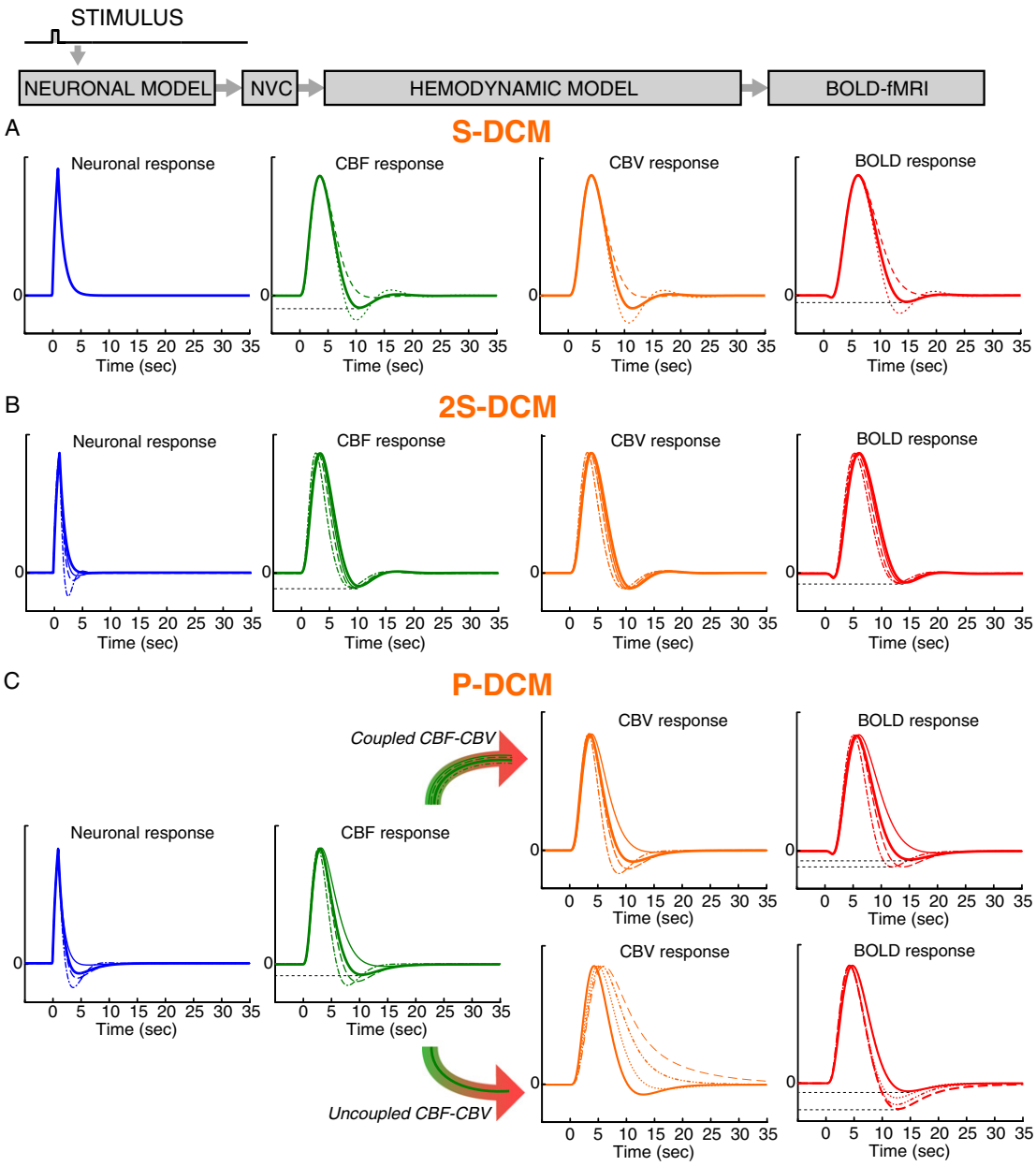

Fig. 3. Impulse response functions of neuronal, CBF, CBV and BOLD signals to a short stimulation (1 s long) as modeled by different DCMs. (A) Responses modeled by S-DCM, where we have varied the decay parameter of the feedback based NVC (*S1* — solid thick line: $\kappa = 0.64$ Hz; *S3* — dashed line: $\kappa = 0.9$ Hz; *S2* — dotted line: $\kappa = 0.5$ Hz). (B) Responses modeled by 2S-DCM, where we have varied only the inhibitory–excitatory connection of the old two-state neuronal model (*S1* — solid thick line: $\mu = 0.125$ Hz; *S2* — solid thin line: $\mu = 0.35$ Hz; *S3* — dashed line: $\mu = 0.65$ Hz; *S4* — dot-dashed line: $\mu = 1.1$ Hz). (C) Responses modeled by P-DCM, where we first varied only parameters of the adaptive two-state model (*S1* — solid thick line: $(\mu, \lambda) = (1, 0.2)$ Hz; *S2* — solid thin line: $(0.2, 0.2)$ Hz; *S3* — dashed line: $(0.5, 0.15)$ Hz; *S4* — dot-dashed line: $(2, 0.2)$ Hz). The effect of this manipulation on the BOLD response is depicted in the top row. Later we additionally varied the viscoelastic time constant that controls vascular uncoupling (*S1a* — solid line: $\tau = 3$ s; *S1b* — dotted line: $\tau = 8$ s; *S1c* — dot-dashed line: $\tau = 15$ s; *S1d* — dashed line $\tau = 27$ s), where we considered the CBF response depicted with a thick solid line as the input. The effect on the BOLD response is shown in the bottom row. Response amplitudes generated with different sets of parameters are normalized for better visualization of the overall differences.

its dynamics are not further regulated (only its contribution to the excitatory activity via μ).

In Fig. 4B, we can see the effect of neuronal inhibition on the excitatory activity during sustained stimulation that results in adaptively reducing the neuronal activity to its plateau and in a brief deactivation after stimulus cessation. However, the two-state model results in only weak and brief adaptive responses and post-stimulus deactivations. These transients are small compared to the main signal change. This is also true for transients seen in CBF, CBV and BOLD responses, which again originate almost entirely from the feedback based NVC. In general, the range of possible BOLD signal dynamic transients for different neuronal time courses is very restrictive.

P-DCM

In Fig. 3C, neuronal responses produced by the new adaptive two-state model are shown for the short stimulus, where we have varied the values of the inhibitory gain factor λ and the inhibitory–excitatory connection μ. P-DCM effectively models post-stimulus neuronal deactivation, which may vary from weak (or even none) to strong and long lasting. The CBF responses represent only delayed and temporally smoothed versions of the neuronal responses.

The top panel of Fig. 3C shows the CBV and BOLD responses for a tight coupling between CBF and CBV during both steady-state and transient periods; i.e., setting viscoelastic time constant $\tau = 0$ s as in S- and 2S-DCM. In this case, the post-stimulus BOLD undershoot is smaller

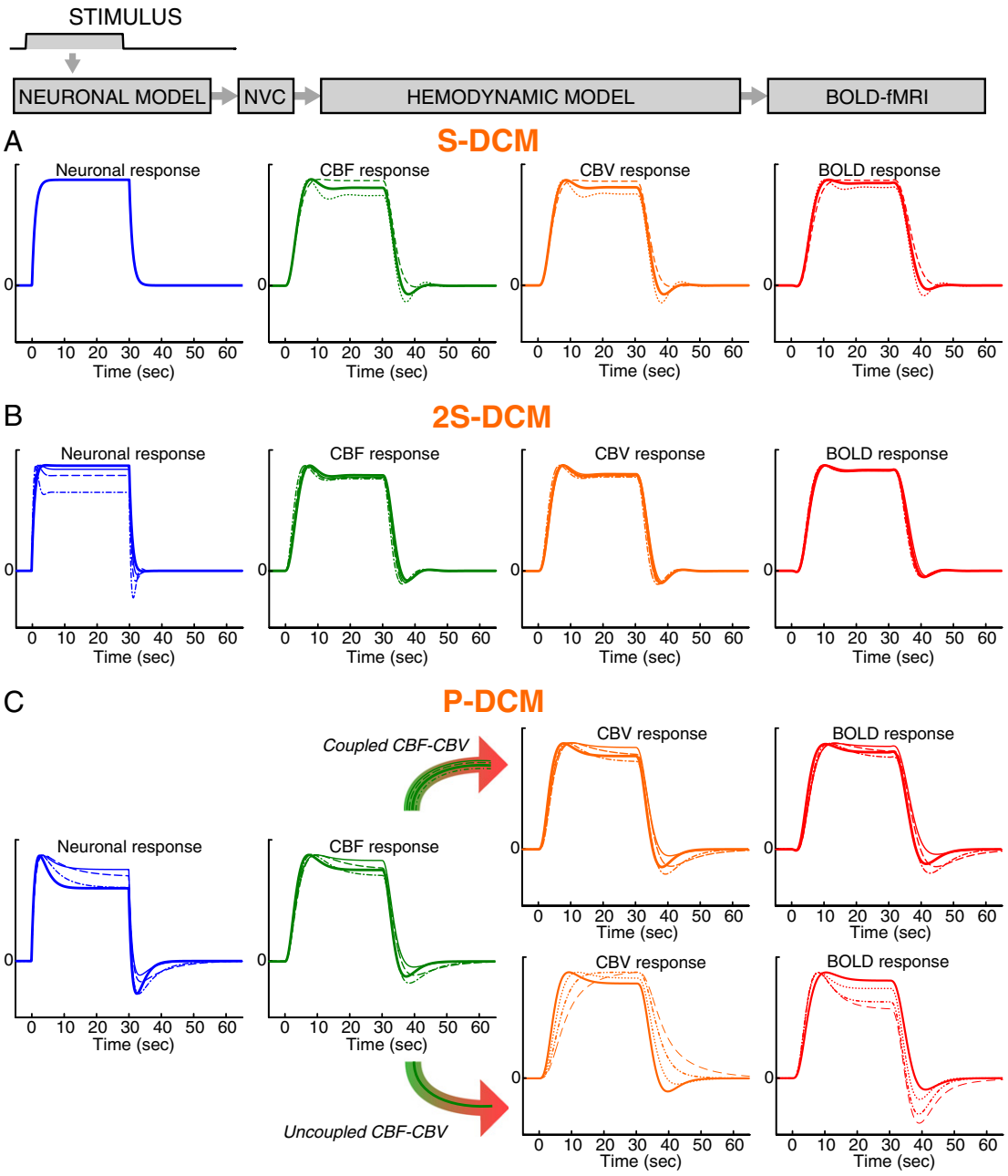

Fig. 4. Responses for neuronal, CBF, CBV and BOLD signals to a 30 s sustained stimulus as modeled by different DCMs. The same parameters as in Fig. 2 were used for S-DCM and 2S-DCM simulations. For P-DCM, slightly different parameter combinations for the neuronal model were used to demonstrate its variability (*S1* — solid thick line: $(\mu, \lambda) = (1, 0.2)$ Hz; solid thin line: $(\mu, \lambda) = (0.3, 0.2)$ Hz; dashed line: $(\mu, \lambda) = (0.35, 0.1)$ Hz; dotted-dashed line: $(\mu, \lambda) = (0.65, 0.1)$ Hz). The response amplitudes generated with different sets of parameters are normalized for better visualization of the overall differences.

than CBF post-stimulus deactivation, in contradiction to e.g. Chen and Pike (2009) or Krüger et al. (1999). Moreover, a difference in post-stimulus undershoots results from neuronal modulation (see e.g. Fig. 5A in Yeşilyurt et al. (2010)). The bottom panel of Fig. 3C shows CBV and the BOLD signal for the case of uncoupling between CBF and CBV during transient periods, i.e. considering viscoelastic time constant $\tau > 0$ s, as in the original balloon model. For simplicity, the value of τ was varied only for one neuronal response input (thick line, left). With larger τ values, the return of CBV response to the baseline becomes slower, which in turn results in stronger post-stimulus BOLD undershoot. In fact, this response combines both a faster component caused by the neuronal signal with a slower component caused by vascular uncoupling (see e.g. Fig. 6A in Kim and Ogawa (2012)).

Fig. 4C displays the neuronal response to sustained stimulation, which exhibits a decrease to steady-state value after an initial overshoot and a post-stimulus undershoot (see e.g. Fig. 18A–D in Logothetis (2002) and Fig. 3A, D, G in Shmuel et al. (2006)). These neuronal transients are again reflected in the CBF, CBV and BOLD responses (see Fig. 4C, top). Both the initial overshoot and the post-stimulus deactivation are reflected in the CBF response, albeit smoothed and attenuated (see e.g. Fig. 5B in Sadaghiani et al. (2009) or Fig. 6C in Huber et al. (2014)). For $\tau = 0$ (top panel), in the BOLD response, these transients are less visible than in CBF and CBV. In contrast, for $\tau > 0$ (bottom panel), the BOLD response exhibits even stronger transients. Note that although both the neuronal activity and the BOLD response have an initial overshoot before settling to a steady-state (which typically is

interpreted as neuronal adaptation), the BOLD response overshoot has both neuronal and vascular contributions, with the latter being the main contributor for large τ values. Importantly, the post-stimulus undershoot in the BOLD response is stronger than in the CBF response, resembling the experimental observations (e.g. see Fig. 3E and F in Chen and Pike (2009)).

Connectivity

Fig. 5 shows the simulation results from the neural network in Fig. 2A for the different DCMs.

S-DCM

For feedforward positive and negative connections, respectively, the single-state neuronal model is able to model both increases and decreases of neuronal activity in the target areas R_2 and R_3 (see Fig. 5, top row). The positive modulation of feedback connection between R_2 and R_1 leads to an increase of neuronal activity and BOLD amplitude in both R_2 and R_1 areas and to decrease of activity in area R_3. While the faster neuronal propagation of the neuronal activity (solid line), generated within the first simulation scenario, still enables the NVC to introduce small transients in the BOLD response, the slower neuronal dynamics (dashed line) cancels its effect, resulting in no over- and undershoot in the BOLD response. The same behavior can also be seen in area R_3 that exhibits neuronal deactivation during the stimulation period.

2S-DCM

The two-state neuronal mechanism employed in 2S-DCM allows the excitatory activity to be locally regulated by the inhibitory activity. While this can introduce small transients at the neuronal level, their presence is barely transferred to the BOLD response (see Fig. 5, middle row). Moreover, in case of slower neuronal dynamics (dashed line), these transients become negligible and BOLD responses are transientless as well. The positive modulation of feedback connection between R_2 and R_1 areas has a very similar effect on the first two areas to that in S-DCM. Most importantly, 2S-DCM is not able to express a decrease of the neuronal activity below the baseline in the R_3 area, because all excitatory connections are positively constrained. As such, 2S-DCM can potentially suffer from very low explained signal variance if both activations and deactivations are present in the measured BOLD signals.

P-DCM

We can see that with positive and negative feedforward connections, respectively, the adaptive two-state neuronal model of P-DCM is able to express both an increase and decrease of neuronal activity in target areas R_2 and R_3 (see Fig. 5, bottom row). In contrast to S- and 2S-DCM, significant neuronal transients are present in cases of both faster (solid line) and slower (dashed line) neuronal dynamics and in the BOLD responses. Practically, the slower neuronal dynamics introduce more delay and smoothness into the observed neuronal and BOLD responses. In this particular setting, all regions exhibit post-stimulus neuronal deactivation and also a post-stimulus BOLD undershoot that has a neuronal origin. Furthermore, the negative response in R_3 first

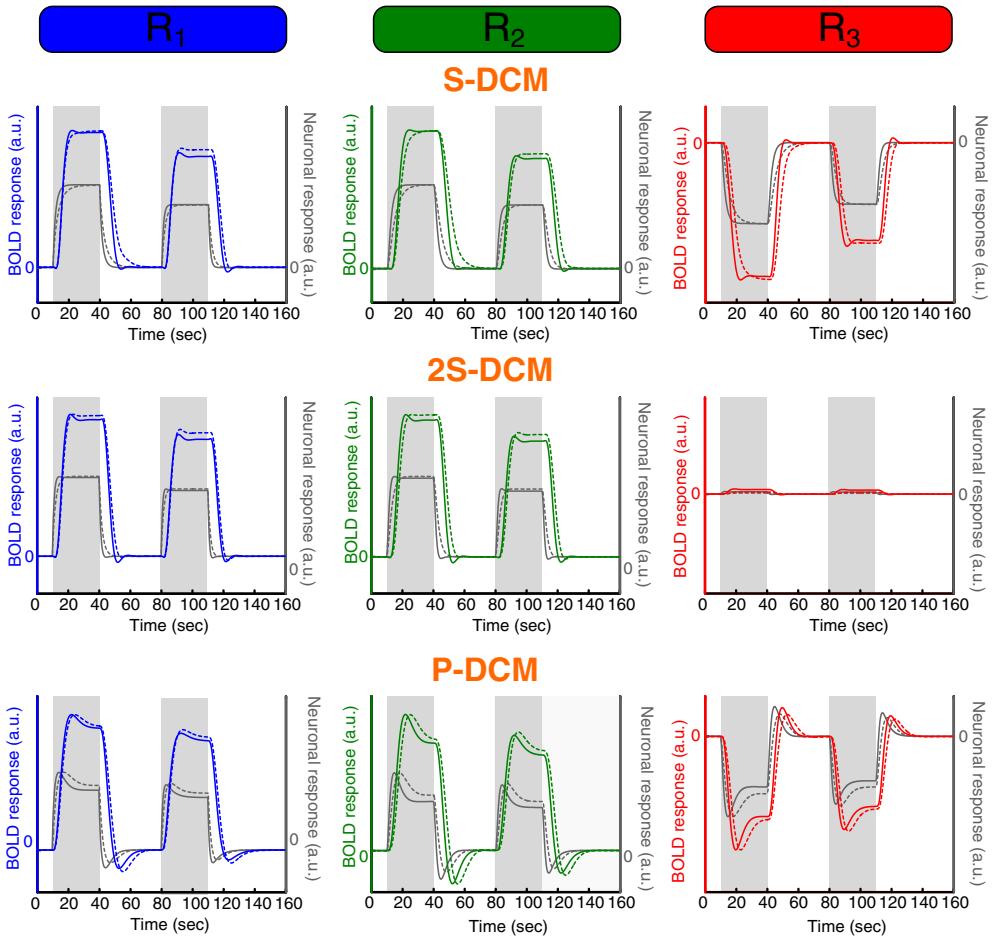

Fig. 5. Dynamics of the neuronal (gray) and BOLD signals (colored) generated via the neural network in Fig. 2 by the different DCMs. Separate columns corresponds to the responses in the three individual areas. Time-courses depicted with a solid line were generated using the first scenario, whereas the time-course generated in the second scenario are depicted with dashed lines. Response amplitudes generated with different sets of parameters are normalized for better visualization of the overall differences.

decreases sharply with stimulus onset and then adaptively increases during stimulation. After stimulation offset, it exhibits an increase of the neuronal activity above the baseline. The associated negative BOLD response initially decreases and is followed by an adaptive increase during the stimulation period and a post-stimulus BOLD overshoot after stimulus offset (examples of these responses in experimental data can be found e.g. in Fig. 3 of Shmuel et al. (2006) or in Fig. 4 of Huber et al. (2014)). This post-stimulus BOLD overshoot mirrors the post-stimulus BOLD undershoot that follows the positive BOLD response. As such, the simulated dynamics of the negative neuronal and BOLD responses are in good agreement with experimental observations obtained with both electrophysiological and fMRI recordings (Huber et al., 2014; Shmuel et al., 2006). The feedback excitatory connection between R_2 and R_1 leads to stronger adaptive neuronal responses during stimulation and post-stimulus deactivation, both reflected in the BOLD responses. Further, note that even though all regions had the same setting of local balance between excitatory and inhibitory neuronal populations, the amplitude of the transient responses varies between regions. This is because the local balance is further disturbed through the remote excitatory connections, which can lead to more pronounced transients — as seen in area R_2.

Experimental data

The results obtained by fitting S-DCM to BOLD data are displayed in Fig. 6A. One can see that fitted BOLD responses (in red) can represent the positive part of the measured signal in terms of the main amplitude change (see Fig. 6A). Modulation of the excitatory self-connection (σ) gained different values for different conditions ($\sigma = 1.10$ during static stimuli, followed by $\sigma = 1.15$ after static stimuli, and $\sigma = 0.33$ during flickering stimuli, followed by $\sigma = 0.65$ after flickering stimuli), but these cannot explain large adaptive profile in measured positive BOLD response during static stimuli and strong post-stimulus BOLD undershoot after flickering stimuli. Further, even though there are small transients present in CBF and BOLD responses especially to static stimuli, these are independent of stimulus type. They are produced by feedback based NVC. These transients are not present in CBF and BOLD responses during flickering stimuli due to smaller $\sigma = 0.33$.

The results of fitted BOLD responses obtained by 2S-DCM are visually quite similar to S-DCM (see Fig. 6B). However, the underlying story at the neuronal level is quite different. Modulation of the inhibitory–excitatory connection during the static condition resulted in a relatively strong contribution of the inhibitory activity to the excitatory activity during both the stimulation and the post-stimulus interval ($\mu = 0.55$ and $\mu = 0.39$ respectively). Nevertheless, these modulations had small effect on transients in CBF and BOLD responses. Transients in modeled CBF and BOLD responses are still mostly generated via negative feedback based NVC and they cannot explain large adaptation in measured positive BOLD response. In the case of the flickering condition, the effect of inhibitory activity is smaller ($\mu = 0.15$), which agrees well with the fact that the plateau of the BOLD response remains relatively flat during the stimulation interval. Although there is stronger involvement of the inhibitory activity ($\mu = 0.85$) during the post-stimulus interval, it has negligible effect on modeled post-stimulus BOLD undershoot and thus the large post-stimulus undershoot in measured BOLD response cannot be explained by this model.

P-DCM provides very accurate fits of the BOLD responses for both experimental conditions (see Fig. 6C). During static stimuli, the neuronal model is capable of representing a large adaptation of the neuronal response through a strong contribution of the inhibitory activity ($\mu = 0.44$) with respect to excitatory-self connection ($\sigma = 0.73$). The

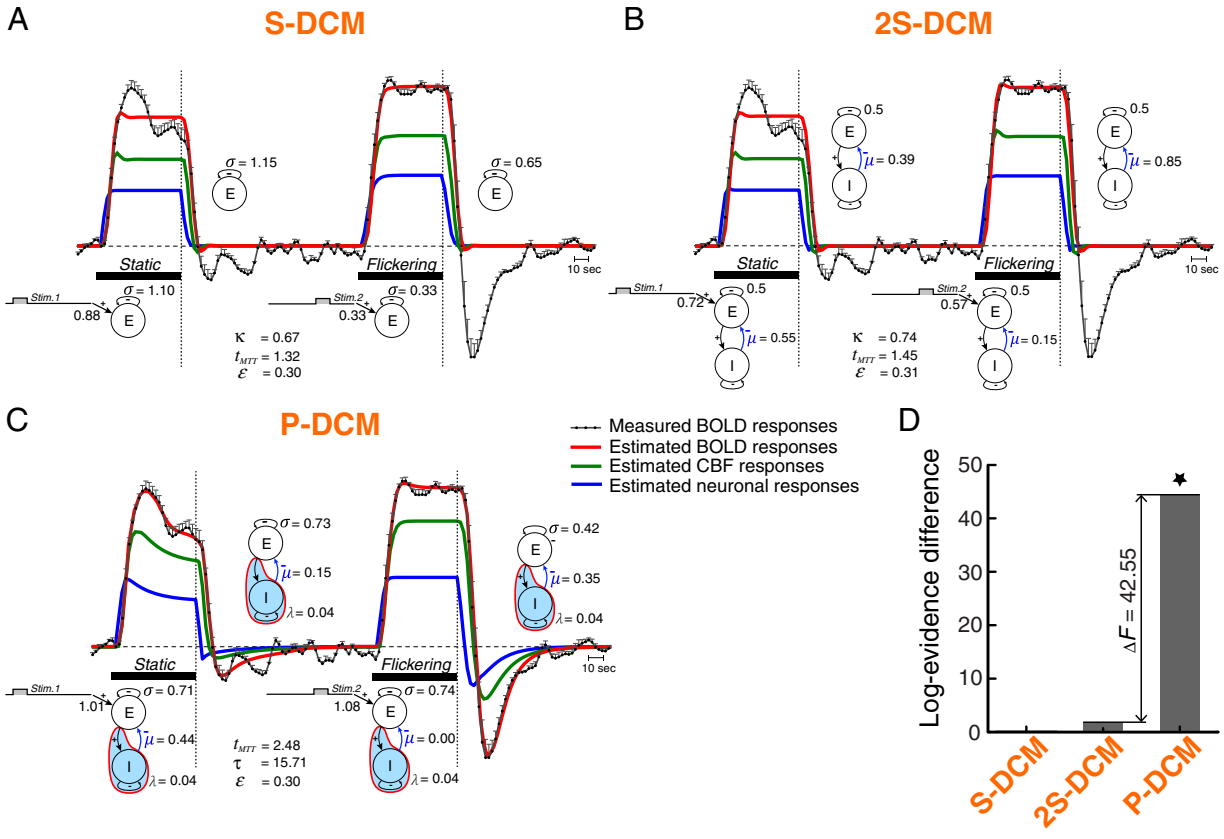

Fig. 6. Results obtained by fitting experimental data by (A) S-DCM, (B) S-DCM and (C) P-DCM. These plots include the estimated neuronal, CBF and BOLD responses (solid lines) from the measured BOLD data (solid line with dots). Their amplitudes are in arbitrary units, scaled for better visual appearance. The error bars around the measured BOLD responses represent the 95% confidence interval. The horizontal bars represent the 55 s of visual stimulation with static and flickering checkerboard, respectively. The model parameters are listed with their estimated values. (D) Results of the Bayesian model comparison based on the model log-evidence difference (with respect to S-DCM which scored the lowest log-evidence), with a star marking the winning model.

inhibitory activity by itself exhibits slower temporal dynamics (not shown) controlled by the inhibitory gain factor ($\lambda = 0.04$). Thus, the adaptive profile of the observed BOLD response mainly has a neuronal origin. Next, during the post-stimulus interval, the excitatory self-connection is about the same as during the stimulation interval ($\sigma = 0.73$) but the contribution of inhibitory activity is smaller ($\mu = 0.15$). This results in a small (but prolonged) neuronal post-stimulus deactivation. This neuronal deactivation is also reflected in the CBF response and contributes to the post-stimulus BOLD undershoot. Additional contribution to the small post-stimulus BOLD undershoot is caused by vascular uncoupling ($\tau = 15.71$ s). During flickering stimuli, we can see that there is no contribution of the inhibitory activity to neuronal response ($\mu = 0.00$); i.e. the profile of positive response during flickering stimuli is defined by excitatory activity only $\sigma = 0.74$, which is about the same as during static stimuli. Although modeled neuronal and CBF responses (displayed in blue and green, respectively) show flat plateau, the positive BOLD response exhibits small overshoot due to the vascular uncoupling. Note that the vascular uncoupling is constant over all stimulus and post-stimulus intervals (estimated $\tau = 15.71$ s). Finally, during the post-stimulus interval, the excitatory self-connection is smaller ($\sigma = 0.44$) and the contribution of inhibitory activity is increased ($\mu = 0.35$), causing strong and long lasting post-stimulus neuronal deactivation. This post-stimulus deactivation is reflected in CBF response and represents the main contribution to the post-stimulus BOLD undershoot. Overall, in this experimental example, the transients seen during the static and flickering stimulations (i.e. adaptation during stimulation for static and post-stimulus undershoot for flickering) are dominated by the neuronal processes. It is important to realize that modeled neuronal dynamics during post-stimulus intervals still reflect properties of presented stimuli and that they can exhibit large differences dependent on stimulus type, resulting in broad variation of very small to very large post-stimulus BOLD undershoot.

Quantitative evaluation of the three DCMs using Bayesian model comparison based on log-evidence difference (Fig. 6D) suggests positive evidence that 2S-DCM is better than S-DCM (with $\Delta F = 1.55$ that corresponds to Bayes factor of 4.7 (Kass and Raftery, 1995)) and very strong evidence that P-DCM is superior to 2S-DCM (with $\Delta F = 42.55$ that corresponds to Bayes factor of $\sim 3.0 \cdot 10^{18}$). Note that P-DCM is selected as a clear winning model even though its complexity (i.e. the number of free parameters) is about twice as high as the complexity of S-DCM or 2S-DCM in this case.

Discussion

In this paper, we have introduced a new generative model for the fMRI signal inspired by existing experimental data on neuronal activity, neurovascular coupling, hemodynamics and fMRI physics (listed in the Introduction section). This novel physiological framework was applied to DCM of fMRI data (P-DCM), which updates previous DCMs using current ideas about the physiological underpinnings of the BOLD signal. P-DCM models the hemodynamic response to changes in neuronal activity as a chain of causal processes: the balance between excitatory and inhibitory neurons drives the neurovascular coupling which induces changes in CBF in a strictly feedforward manner. The oxygen metabolism, although mechanistically independent from the CBF response, is tightly related to the CBF. Changes in CBF trigger changes in (venous) CBV. Due to the biomechanical properties of blood vessels, CBV can have a different time course than the CBF during the transient states (as described by the original balloon and Windkessel models). Note that although CBF and CBV are causally linked, their dynamics can be different, which is often referred to as "uncoupling". The BOLD signal then reflects both transient and steady-states originating in both ('active') neuronal (E–I balance) and ('passive') vascular dynamics. Last but not least, at the neuronal level, the long-range extrinsic connections communicate via excitatory projection neurons between different cortical areas in a way that accounts for both neuronal activations and deactivations.

P-DCM represents a fundamental departure from current DCM models (S-DCM and 2S-DCM) used in fMRI analysis. The critical distinction between P-DCM, on the one hand, and S-DCM and 2S-DCM, on the other hand, is that P-DCM is also concerned with modeling dynamic transients between steady-states, while S-DCM and 2S-DCM are mainly concerned with modeling amplitude changes between baseline and activation states. In a subsequent paper, we will show that accurately modeling the BOLD signal transients also affects connectivity parameter estimates.

Maintaining E–I balance is essential for normal brain functioning. For instance, if the inhibitory neurons are blocked pharmacologically, cortical activity can become epileptic (Dichter and Ayala, 1987). The neuronal transients originate in a temporary loss of balance between excitatory and inhibitory populations (Haider et al., 2006). It is now generally believed that modeling E–I balance – as an underlying source of the BOLD response (Logothetis, 2008) – is crucial for relating the neuronal and hemodynamic responses. It has been suggested that neuronal transients (i.e. initial overshoot and post-stimulus deactivation) can reflect the number and type of activated cells, i.e. the neuronal preference, in stimulus processing (Krekelberg et al., 2006). Importantly, it has also been shown that neuronal transients are reflected in the BOLD response (Logothetis, 2008; Shmuel et al., 2006) and that their changes can modulate the BOLD signal post-stimulus undershoot (Mullinger et al., 2013; Sadaghiani et al., 2009). We were able to demonstrate that our new adaptive two-state model can generate a large repertoire of neuronal responses to both short and sustained stimuli (Figs. 3 and 4). This allows it to model neuronal responses with an initial peak followed by a decay to a lower steady-state plateau level and post-stimulus deactivation — as commonly observed in experimental data. Moreover, the new model also facilitates modeling of negative neuronal responses with shapes similar to the experimental observations (Huber et al., 2014; Mullinger et al., 2014; Shmuel et al., 2006).

In accordance with recent observations that neurovascular coupling is mediated by a feedforward mechanism (Attwell et al., 2010; Devor et al., 2007; Lauritzen, 2005), we have proposed a new NVC model that is strictly feedforward in nature. This feedforward NVC in P-DCM was designed to transpose the neuronal transients into the CBF response. In contrast, the NVC in S-DCM and 2S-DCM involves CBF feedback introducing CBF transients not present in the neuronal activity. Since different neuronal properties can be distinguishable – especially during transient periods between steady-states (by comparing adaptive profiles or post-stimulus deactivations) – the feedforward mechanism can, in principle enable the characterization of E–I balance through non-invasive hemodynamic signals (Boynton et al., 1996; Hoge et al., 1999; Sadaghiani et al., 2009). In Figs. 3–5, we have shown that in P-DCM the neuronal transients, such as initial overshoot or post-stimulus deactivation, are reflected in the CBF response, and that they can contribute significantly to the dynamic transients observed in the BOLD response. This is an important departure from the previous DCM models, where neuronal transients (if generated locally) do not contribute much to the BOLD response overshoot and undershoot.

In addition to the transient responses of neuronal origin, the BOLD response can also exhibit transients mainly originating from vascular uncoupling between CBF and CBV. Here, during transient periods, CBV lags after CBF, which introduces an additional overshoot and post-stimulus undershoot into the BOLD response. Although this phenomenon is consistently observed in experimental data that measure CBV, CBF and BOLD signal (Chen and Pike, 2009; Huber et al., 2014; Kim and Ogawa, 2012; Mandeville et al., 1998), standard DCM models do not take this physiological effect into account. In P-DCM, we incorporated this additional mechanism,

which enables modeling both the active neuronal and the passive vascular contributions to BOLD response transients.

Our results obtained through simulations and by fitting P-DCM to experimental data predict that if the vascular effect is present together with the neuronal transients, then the CBF response will exhibit weaker and shorter post-stimulus deactivation than the BOLD post-stimulus undershoot. That is, even in the case of no CBF post-stimulus deactivation, there can still be a post-stimulus BOLD undershoot, caused solely by vascular uncoupling (e.g. Sadaghiani et al. (2009), Krüger et al. (1999)). Similarly, if there is post-stimulus deactivation in CBF, which is larger than, or comparable to, the size of BOLD post-stimulus undershoot, then the post-stimulus BOLD undershoot is caused solely by neuronal deactivation or together with a minimal contribution from vascular uncoupling. In the latter case, there would also be a clear post-stimulus undershoot in the CBV response. In all cases, the size of post-stimulus BOLD undershoot also scales with the stimulus duration. All these properties of our model are in good agreement with experimental observations (Donahue et al., 2009; Huber et al., 2014; Kim and Ogawa, 2012). Note that the initial overshoot in the BOLD response during stimulation can have both neuronal and vascular contribution, which can be sometimes misinterpreted to be solely related to neuronal adaptation. Finally, in the Supplementary Material S4, we show that the size of BOLD transients caused by vascular uncoupling can increase with stronger magnetic fields and with larger α values (defining the steady-state CBF–CBV relationship).

The neuronal connectivity model employed in P-DCM combines the properties of the single-state and standard two-state models: (1) we kept the simple mechanism employed in S-DCM to express both the increase and decrease of neuronal activity around the baseline, by allowing connections with both positive and negative effects; and (2) as in 2S-DCM, we consider the excitatory activity as being locally regulated by inhibitory activity and extrinsic connections are made between the excitatory units; however, with additional (local) control over the balance between excitatory and inhibitory activity. In contrast to the previous models, we also introduced additional possibility of modulation of all intrinsic connections — that could be employed if there is interest in comparing neuronal transients (i.e. adaptive profile and post-stimulus deactivation) between different experimental conditions (see below). We have illustrated the properties of the P-DCM connectivity model on a simple three-node network example. There we have shown that in contrast to S- and 2S-DCM, within the network of brain areas, P-DCM can produce significant dynamic transients in both positive and negative BOLD responses that are commonly observed in fMRI data (Huber et al., 2014; Shmuel et al., 2006). This example does not cover all possible scenarios and does not provide a complete comparison of different models. For instance, we did not include cases where S-DCM employs a negative (feedback) connection between two regions, which can introduce transients in the neuronal responses. As a matter of fact, the neuronal model in P-DCM considers both local (through inhibition) and remote (through negative connections that are not necessarily related to neuronal inhibition) causes of neuronal activity decreases. Whether local or remote mechanisms are more involved in adapting the neuronal response during stimulation and post-stimulus interval depends on experimental conditions, since both are physiologically plausible.

BOLD-fMRI experimental data served to further demonstrate qualitative and quantitative differences between P-DCM and other two DCMs in application to single ROI responses. Using modulation of excitatory self-connection and inhibitory–excitatory connection together with globally estimated inhibitory gain factor and viscoelastic time constant, P-DCM accurately fitted response transients during visual stimulations. This experimental data provides direct evidence that it is necessary to consider both active neuronal and passive vascular causes of the BOLD response transients. The model comparison unveiled that S-DCM and 2S-DCM have much lower model evidence mainly because they lack the very basic physiological mechanisms behind the response transients, which makes these models rather unphysiological. From a quantitative perspective, Bayesian model comparison showed that P-DCM is in this case clearly the winning model compared to S-DCM and 2S-DCM.

Nevertheless, P-DCM is still a simplified biophysical model of brain tissue processes, and therefore cannot capture all experimentally observed physiological effects of the underlying neuronal, metabolic and vascular processes. However, we have included the most common effects that are observed in fMRI data and modeled them with an adequate level of simplification given the physiological information content of fMRI data. Importantly, the complexity of the model is tailored so it can be inverted effectively (i.e. preclude overfitting) and remains identifiable (i.e. preclude large posterior parameter correlations).

Limitations and constraints

1. In P-DCM, we have abolished the negative feedback in the neurovascular coupling to eliminate transients in CBF not present in neuronal activity (even though there might be some cases outside of normal human physiology where the feedback based NVC occurs). That is, CBF represents a positively constrained convolution of neuronal activity, resulting in CBF being a smoothed version of neuronal activity. However, we note that there are also some observations that the CBF signal exhibits oscillations that are independent of variations induced by evoked neuronal activity. These slow fluctuations (~ 0.1 Hz), sometimes called Mayer waves, have been attributed to mechanisms such as blood pressure feedback from baroreceptors or spontaneous neurogenic mechanisms (Morris et al., 2010; Ress et al., 2009). Note that these Mayer waves were also part of a working hypothesis to motivate the feedback based NVC used in S- and 2S-DCM (Friston et al., 2000). In principle, this independent vasomotor component of the CBF response could be additionally modeled, however there is no evidence that this vasomotor signal contributes to undershoot of the induced BOLD response.
2. We assumed in P-DCM, as in standard DCM, that the CBF and $CMRO_2$ are tightly coupled during both steady-state and transient periods, as suggested by the oxygen limitation model (Buxton and Frank, 1997) and experimental observations (Nagaoka et al., 2006; Sheth et al., 2004; Zappe et al., 2008a). However, as the NVC is not primarily driven by metabolic demand and metabolic by-products but by neuromediators, oxygen metabolism (or oxygen extraction from the blood, to be precise) and CBF might have different dynamical properties. This has been suggested, for example, by Lu et al. (2004) and van Zijl et al. (2012) as a mechanism for the post-stimulus BOLD undershoot. However, as the effect of CBV and $CMRO_2$ are exchangeable with respect to the BOLD signal dynamics, we argue that for modeling purposes, it is sufficient to consider only one of these two physiological mechanisms. Note that it is currently not technically possible to measure $CMRO_2$ changes directly with a high temporal resolution (but see Vazquez et al. (2012) for a promising approach). Thus, all fMRI results reporting delayed recovery of $CMRO_2$ – as a contributor to the post-stimulus BOLD undershoot – are based on indirect evidence rather than direct observations.
3. In P-DCM, both CBF and $CMRO_2$ are driven by excitatory neuronal activity, which reflects E–I balance (since excitatory activity induces inhibitory activity, which in turn, suppresses excitatory activity). However, there is also a recent 'speculative hypothesis' (see Buxton et al. (2014) and references therein) that the coupling ratio between CBF and $CMRO_2$ is sensitive to different aspects of neuronal activity. For example, if there is a strong

involvement of inhibitory activity, CBF increases more relative to $CMRO_2$ because of the vasodilatory effect of the inhibitory mechanisms. If established, this additional mechanism could be incorporated in the future in P-DCM through modulation of the coupling ratio of CBF and $CMRO_2$ by inhibitory activity.

4. We assume a power-law relationship between CBF and CBV during the steady-state: $CBV = CBF^{\alpha}$, with α being fixed to 0.32 as in other DCMs for fMRI, which is slightly lower than the original value ($\alpha = 0.38$) estimated by Grubb et al. (1974). This assumption means that a CBF increase of 50% corresponds to a CBV increase of about 12% (see also Appendix A). However, one should be aware that there is still no consensus about this value. For instance, in the human brain, Chen and Pike (2010) estimated a substantially lower ($\alpha = 0.18$), whereas others report values in the range 0.29–0.64 (Rostrup et al., 2005). In the anesthetized animal brain, reported values are in the range 0.24–0.38 (Lu et al., 2009). A recent study by van Raaij et al. (2012) indicates a similar α value as Grubb et al. (1974) in cortical gray matter, but a significantly different value ($\alpha = 0.75$) in subcortical gray matter. In general, it is expected that in the initial phase of the hemodynamic response and for short stimulus durations, the largest portion of CBV changes occurs at the level of arteries/arterioles; i.e., CBV changes less with respect to CBF (smaller α) (Kim and Kim, 2011; Vanzetta et al., 2005). However, for longer stimulus duration, the venous CBV changes start playing a more significant role, so the CBV changes more with respect to CBF (higher α), accompanied by a slower rise and decay time constants. Increasing α also increases the degree of nonlinearity in the flow-volume behavior. By considering the value of 0.32, we are around the middle of the range of reported values, which should be suitable for common stimulus durations and it makes the hemodynamic model only mildly nonlinear. Nevertheless, all models can easily incorporate other values of α (see e.g. Supplementary Material S4).
5. We have made several assumptions regarding the flexibility of our model. Parameters controlling the delay and smoothness of CBF response to neuronal activation were considered fixed in the new NVC for the simulations of the experimental data (adjusted to produce ~3 s delay in the case of a short stimulus). Although we do not expect these parameters to vary much in healthy brains, in the diseased brain the vascular regulatory mechanisms are potentially altered, which could require a different parameterization of the NVC (Iadecola, 2004). In general, it does not seem reasonable to allow larger variance of these parameters if we rely only on BOLD data, because their changes would be correlated with changes of the mean transit time (t_{MTT}) and partly with the viscoelastic time constant (τ). However, the correlated effects of these parameters on the predicted BOLD response could be constrained using ASL data, which allows a simultaneous measurement of CBF and BOLD signals. Similarly, if we rely only on the BOLD signal, we might sometimes run into identifiability problems between the parameters controlling neuronal transients (μ, λ) and the τ parameter controlling the vascular uncoupling, because (in certain ranges) these mechanisms can produce a similar BOLD undershoot. Also in this case, the identifiability should be greatly improved using ASL data, or by experimentally modulating the neuronal transients. We will examine this issue in a following paper.
6. Considering the model complexity, S-DCM and 2S-DCM are equipped with the following free (intrinsic) parameters: one parameter in the neuronal models (σ in S-DCM and μ in 2S-DCM); one parameter in the feedback based NVC (κ); one parameter in the hemodynamic model (t_{MTT}); and one parameter in the BOLD signal model (ε). That is, in total four region-specific parameters are utilized to adjust the dynamics of the BOLD response. In contrast, in P-DCM we assume the following free parameters: three parameters in the adaptive two-state neuronal model (σ, μ, λ); zero parameters in the new NVC; two parameters in hemodynamic model (t_{MTT}, τ); and one parameter in the BOLD signal model (ε) — in total, six free parameters. However, the excitatory self-connection σ is considered global, so in terms of connectivity analysis, it will not multiply by the number of ROIs. Moreover, since the strengths of the other neuronal parameters (μ, λ) are relative to σ (see Supplementary Material S1), it could be that in the future we will be able to identify functional dependencies between these parameters and slightly reduce the number of free neuronal parameters in P-DCM. Furthermore, the intra- to extra-vascular ratio ε could be fixed as well, given a more accurate parameterization of the BOLD equation for a given field strength. Note that the responses in Figs. 3C–4C were generated by varying only three parameters (two neuronal and one viscoelastic time constant) demonstrating the great flexibility of the P-DCM model, but for regular data fitting (model inversion) we must also fit the mean transit time t_{MTT}. Therefore, the P-DCM can account for large variations in the BOLD signal by using four free parameters. Nevertheless, in the experimental example above, we have shown, that despite the increase in complexity, P-DCM has higher model evidence than S-DCM and 2S-DCM.

Future prospects

In this paper, we have focused on the theoretical motivation and phenomenology of the new P-DCM model — and the associated benefits with respect to S-DCM and 2S-DCM. The analysis of experimental data served as an illustrative example, demonstrating the utility for further application. In a subsequent paper, we will provide a detail statistical evaluation of these models, based on Bayesian model comparison (Penny et al., 2010), applied to networks of multiple brain areas of fMRI data. Experimental fMRI data will be used to show in detail that the new model provides a better explanation of observed physiological responses, especially in the context of multimodal imaging. Currently, we are testing P-DCM on simultaneous electrophysiological recordings of neuronal activity and the BOLD signal and on simultaneous measurements of CBF, CBV and BOLD signals. In the future, we will extend this model to other fMRI measurements such as ASL that measures both CBF and BOLD signal, and vascular space occupancy (VASO) that measures both CBV and BOLD signal.

Summary

DCM is a widely used approach for inferring effective connectivity in neuronal networks from measured fMRI data. The generative model can also be used to deconvolve a single ROI or voxel time-course. However, until now, DCM variants relied on simplistic assumptions about the physiological link between the neuronal and BOLD responses. In this paper, we have presented a more informed physiological framework for DCM; namely, P-DCM, inspired by many recent experimental observations. P-DCM includes basic physiological mechanisms that are necessary to account for the wide repertoire of measured BOLD responses that are modeled insufficiently by previous models. The dynamic BOLD responses may provide a window on the underlying neuronal and hemodynamic processes, provided they can be modeled adequately. P-DCM allows for a comprehensive modeling of the neuronal and vascular processes, and offers a new way of inferring changes in neuronal activity and effective connectivity from fMRI signals.

Acknowledgments

This work was financially supported by the Marie Curie Initial Training Network grant (PITN-GA-2009-238593) of EU and VIDI grant (452-11-002) of the Netherlands Organization for Scientific Research (NWO). KF was funded by the Wellcome Trust. All authors report no (financial) conflicts of interest.

Appendix A

Table A.1
Parameter values intrinsic neuronal connections, neurovascular coupling, and hemodynamic model used for single-ROI simulations.

	S-DCM			2-DCM				P-DCM							
	Short & long			Short & long				Short				Long			
	S1	S2	S3	S1	S2	S3	S4	S1	S2	S3	S4	S1	S2	S3	S4
Neuronal model															
σ (Hz)	1	1	1	0.5	0.5	0.5	0.5	1	1	1	1	1	1	1	1
μ (Hz)	–	–	–	0.125	0.35	0.65	1.1	0.8	0.2	0.5	2	1	0.3	0.35	0.65
λ (Hz)	–	–	–	–	–	–	–	0.2	0.2	0.15	0.2	0.2	0.2	0.1	0.1
Neurovascular coupling															
κ (Hz)	0.64	0.5	0.9	0.64	0.64	0.64	0.64	–	–	–	–	–	–	–	–
$\gamma = 0.32$ Hz (both S-DCM and 2S-DCM)															
$\varphi = 0.6$ Hz, $\chi = 1.5$ Hz, $\phi = 0.6$ Hz (P-DCM)															
Hemodynamic model															
$\alpha = 0.32$, $t_{MTT} = 2$ s, $E_0 = 0.4$ (same for S-DCM, 2S-DCM and P-DCM)															
$\tau = 0$ s (P-DCM: S1-S4 for both short and long stimuli),															
S1a: $\tau = 3$ s, S1b: $\tau = 8$ s, S1c: $\tau = 15$ s, S1d: $\tau = 27$ s (P-DCM for both short and long stimuli)															
S-DCM: S1 – solid thick line; S2 – dotted line; S3 – dashed line.															
2S-DCM: S1 – solid thick line; S2 – solid thin line; S3 – dashed line; S4 – dot-dashed line.															
P-DCM: S1 – solid thick line; S2 – solid thin line; S3 – dashed line; S4 – dot-dashed line; S1a – solid thick line;															
S1b – dotted line; S1c – dot-dashed line; S1d – dashed line.															

Table A.2
Parameter values of intrinsic neuronal connections, neurovascular coupling, and hemodynamic model used in connectivity simulations reported in Fig. 5.

	S-DCM						2S-DCM						P-DCM					
	Slow			Fast			Slow			Fast			Slow			Fast		
	R1	R2	R3	R1	R2	R3	R1	R2	R3	R1	R2	R3	R1	R2	R3	R1	R2	R3
Neuronal model																		
σ (Hz)	0.5	0.5	0.5	1	1	1	0.5	0.5	0.5	1	1	1	0.5	0.5	0.5	1	1	1
μ (Hz)	–	–	–	–	–	–	0.125	0.125	0.125	0.25	01.25	0.25	0.2	0.2	0.2	0.4	0.4	0.4
λ (Hz)	–	–	–	–	–	–	–	–	–	–	–	–	0.15	0.15	0.15	0.15	0.15	0.15
Neurovascular coupling																		
$\kappa = 0.64$ Hz, $\gamma = 0.32$ Hz (both S-DCM and 2S-DCM)																		
$\varphi = 0.6$ Hz, $\chi = 1.5$ Hz, $\phi = 0.6$ Hz (P-DCM)																		
Neurovascular coupling																		
$\alpha = 0.32$, $t_{MTT} = 2$ s, $E_0 = 0.4$ (all S-DCM, 2S-DCM and P-DCM)																		
$\tau = 0$ s (P-DCM)																		
Slow – dashed line; *Fast* – solid line.																		

Appendix B. Supplementary data

Supplementary data to this article can be found online at http://dx.doi.org/10.1016/j.neuroimage.2015.07.078.

References

Attwell, D., Iadecola, C., 2002. The neural basis of functional brain imaging signals. Trends Neurosci. 25, 621–625.

Attwell, D., Buchan, A.M., Charpak, S., Lauritzen, M., MacVicar, B.A., Newman, E.A., 2010. Glial and neuronal control of brain blood flow. Nature 468, 232–243 (ST — Glial and neuronal control of brain).

Bandettini, P.A., Kwong, K.K., Davis, T.L., Tootell, R.B.H., Wong, E.C., Fox, P.T., Belliveau, J.W., Weisskoff, R.M., Rosen, B.R., 1997. Characterization of cerebral blood oxygenation brain activation. 109 pp. 93–109.

Biswal, B., Yetkin, F.Z., Haughton, V.M., Hyde, J.S., 1995. Functional connectivity in the motor cortex of resting human brain using echo-planar MRI. Magn. Reson. Med. 34, 537–541 (ST - Functional connectivity in the motor).

Boynton, G.M., Engel, S.A., Glover, G.H., Heeger, D.J., 1996. Linear systems analysis of functional magnetic resonance imaging in human V1. J. Neurosci. 16, 4207–4221 (ST — Linear systems analysis of functio).

Brown, G.G., Eyler Zorrilla, L.T., Georgy, B., Kindermann, S.S., Wong, E.C., Buxton, R.B., 2003. BOLD and perfusion response to finger-thumb apposition after acetazolamide administration: differential relationship to global perfusion. J. Cereb. Blood Flow Metab. 23, 829–837.

Buxton, R.B., 2012. Dynamic models of BOLD contrast. NeuroImage 62, 953–961.

Buxton, R.B., Frank, L.R., 1997. A model for the coupling between cerebral blood flow and oxygen metabolism during neural stimulation. J. Cereb. Blood Flow Metab. 17, 64–72.

Buxton, R.B., Miller, K., Frank, L.R., Wong, E.C., 1998a. BOLD signal dynamics: the balloon model with viscoelastic effects. Proceeding of ISMRM conference. 1.

Buxton, R.B., Wong, E.C., Frank, L.R., 1998b. Dynamics of blood flow and oxygenation changes during brain activation: the balloon model. Magn. Reson. Med. 39, 855–864 (ST — Dynamics of blood flow and oxygenati).

Buxton, R.B., Uludag, K., Dubowitz, D.J., Liu, T.T., 2004. Modeling the hemodynamic response to brain activation. NeuroImage 23, S220–S233 (ST — Modeling the hemodynamic response).

Buxton, R.B., Griffeth, V.E.M., Simon, A.B., Moradi, F., Shmuel, A., 2014. Variability of the coupling of blood flow and oxygen metabolism responses in the brain: a problem for interpreting BOLD studies but potentially a new window on the underlying neural activity. Front. Neurosci. 8, 139-139.

Cauli, B., Hamel, E., 2010. Revisiting the role of neurons in neurovascular coupling. Front. Neuroenerg. 2, 9-9.

Cauli, B., Tong, X.-K., Rancillac, A., Serluca, N., Lambolez, B., Rossier, J., Hamel, E., 2004. Cortical GABA interneurons in neurovascular coupling: relays for subcortical vasoactive pathways. J. Neurosci. Off. J. Soc. Neurosci. 24, 8940–8949.

Chen, J.J., Pike, G.B., 2009. Origins of the BOLD post-stimulus undershoot. NeuroImage 46, 559–568.

Chen, J.J., Pike, G.B., 2010. MRI measurement of the BOLD-specific flow-volume relationship during hypercapnia and hypocapnia in humans. NeuroImage 53, 383–391.

Daunizeau, J., Friston, K.J., Kiebel, S.J., 2009. Variational Bayesian identification and prediction of stochastic nonlinear dynamic causal models. Physica D 238, 2089–2118 (ST — Variational Bayesian identificatio).

Devor, A., Tian, P., Nishimura, N., Teng, I.C., Hillman, E.M.C., Narayanan, S.N., Ulbert, I., Boas, D.a., Kleinfeld, D., Dale, A.M., 2007. Suppressed neuronal activity and concurrent arteriolar vasoconstriction may explain negative blood oxygenation level-dependent signal. J. Neurosci. Off. J. Soc. Neurosci. 27, 4452–4459.

Dichter, M., Ayala, G., 1987. Cellular mechanisms of epilepsy: a status report. Science 237, 157–164.

Donahue, M.J., Stevens, R.D., de Boorder, M., Pekar, J.J., Hendrikse, J., van Zijl, P.C.M., 2009. Hemodynamic changes after visual stimulation and breath holding provide evidence for an uncoupling of cerebral blood flow and volume from oxygen metabolism. J. Cereb. Blood Flow Metab. 29, 176–185.

Fox, M.D., Snyder, A.Z., Vincent, J.L., Corbetta, M., Van Essen, D.C., Raichle, M.E., 2005. The human brain is intrinsically organized into dynamic, anticorrelated functional networks. Proc. Natl. Acad. Sci. U. S. A. 102, 9673–9678.

Frahm, J., Krüger, G., Merboldt, K.D., Kleinschmidt, a., 1996. Dynamic uncoupling and recoupling of perfusion and oxidative metabolism during focal brain activation in man. Magn. Reson. Med. 35, 143–148.

Fransson, P., 2005. Spontaneous low-frequency BOLD signal fluctuations: an fMRI investigation of the resting-state default mode of brain function hypothesis. Hum. Brain Mapp. 26, 15–29.

Friston, K.J., 1994. Functional and effective connectivity in neuroimaging: a synthesis. Hum. Brain Mapp. 2, 56–78 (ST — Functional and effective connectivity).

Friston, K.J., Mechelli, A., Turner, R., Price, C.J., 2000. Nonlinear responses in fMRI: the Balloon model, Volterra kernels, and other hemodynamics. NeuroImage 12, 466–477 (ST — Nonlinear responses in fMRI: the Bal).

Friston, K.J., Harrison, L., Penny, W., 2003. Dynamic causal modelling. NeuroImage 19, 1273–1302 (ST — Dynamic causal modelling).

Friston, K., Mattout, J., Trujillo-Barreto, N., Ashburner, J., Penny, W., 2007. Variational free energy and the Laplace approximation. NeuroImage 34, 220–234.

Friston, K.J., Trujillo-Barreto, N., Daunizeau, J., 2008. DEM: a variational treatment of dynamic systems. NeuroImage 41, 849–885 (ST — DEM: a variational treatment of dyna).

Friston, K.J., Stephan, K.E., Daunizeau, J., 2010. Generalised filtering. Math. Probl. Eng. 2010.

Friston, K.J., Kahan, J., Biswal, B., Razi, A., 2014. A DCM for resting state fMRI. NeuroImage 94, 396–407.

Gordon, G.R.J., Choi, H.B., Rungta, R.L., Ellis-Davies, G.C.R., MacVicar, B.a., 2008. Brain metabolism dictates the polarity of astrocyte control over arterioles. Nature 456, 745–749.

Grubb, R.L., Raichle, M.E., Eichling, J.O., Ter-Pogossian, M.M., 1974. The effects of changes in $PaCO_2$ cerebral blood volume, blood flow, and vascular mean transit time. Stroke 5, 630–639.

Haider, B., Duque, A., Hasenstaub, A.R., McCormick, D.a., 2006. Neocortical network activity in vivo is generated through a dynamic balance of excitation and inhibition. J. Neurosci. Off. J. Soc. Neurosci. 26, 4535–4545.

Havlicek, M., Friston, K.J., Jan, J., Brazdil, M., Calhoun, V.D., 2011. Dynamic modeling of neuronal responses in fMRI using cubature Kalman filtering. NeuroImage 56, 2109–2128.

Hoge, R.D., Atkinson, J., Gill, B., Crelier, G.R., Marrett, S., Pike, G.B., 1999. Stimulus-dependent BOLD and perfusion dynamics in human V1. NeuroImage 9, 573–585.

Huber, L., Goense, J., Kennerley, A.J., Ivanov, D., Krieger, S.N., Lepsien, J., Trampel, R., Turner, R., Möller, H.E., 2014. Investigation of the neurovascular coupling in positive and negative BOLD responses in human brain at 7 T. NeuroImage 97, 349–362.

Hyder, F., Sanganahalli, B.G., Herman, P., Coman, D., Maandag, N.J.G., Behar, K.L., Blumenfeld, H., Rothman, D.L., 2010. Neurovascular and Neurometabolic couplings in dynamic calibrated fMRI: transient oxidative neuroenergetics for block-design and event-related paradigms. Front. Neuroenerg. 2, 1–11.

Iadecola, C., 2004. Neurovascular regulation in the normal brain and in Alzheimer's disease. Nat. Rev. Neurosci. 5, 347–360.

Kass, R.E., Raftery, A.E., 1995. Bayes factors. J. Am. Stat. Assoc. 90, 773–795 (ST — Bayes factors).

Kim, T., Kim, S.-G., 2011. Temporal dynamics and spatial specificity of arterial and venous blood volume changes during visual stimulation: implication for BOLD quantification. J. Cereb. Blood Flow Metab. 31, 1211–1222.

Kim, S.-G., Ogawa, S., 2012. Biophysical and physiological origins of blood oxygenation level-dependent fMRI signals. J. Cereb. Blood Flow Metab. 32, 1188–1206.

Krekelberg, B., Boynton, G.M., van Wezel, R.J.a., 2006. Adaptation: from single cells to BOLD signals. Trends Neurosci. 29, 250–256.

Krüger, G., Kleinschmidt, A., Frahm, J., 1996. Dynamic MRI sensitized to cerebral blood oxygenation and flow during sustained activation. Magn. Reson. Med. 35, 4.

Krüger, G., Kastrup, a., Takahashi, a., Glover, G.H., 1999. Simultaneous monitoring of dynamic changes in cerebral blood flow and oxygenation during sustained activation of the human visual cortex. Neuroreport 10, 2939–2943.

Lauritzen, M., 2005. Reading vascular changes in brain imaging: is dendritic calcium the key? Nature reviews. Neuroscience 6, 77–85.

Lecrux, C., Toussay, X., Kocharyan, A., Fernandes, P., Neupane, S., Lévesque, M., Plaisier, F., Shmuel, A., Cauli, B., Hamel, E., 2011. Pyramidal neurons are "neurogenic hubs" in the neurovascular coupling response to whisker stimulation. J. Neurosci. Off. J. Soc. Neurosci. 31, 9836–9847.

Li, T.Q., Kastrup, a., Moseley, M.E., Glover, G.H., 2000. Changes in baseline cerebral blood flow in humans do not influence regional cerebral blood flow response to photic stimulation. J. Magn. Reson. Imaging 12, 757–762.

Li, B., Daunizeau, J., Stephan, K.E., Penny, W., Hu, D., Friston, K., 2011. Generalised filtering and stochastic DCM for fMRI. NeuroImage 442–457 (ST — Generalised filtering and stochastic).

Lindauer, U., Leithner, C., Kaasch, H., Rohrer, B., Foddis, M., Füchtemeier, M., Offenhauser, N., Steinbrink, J., Royl, G., Kohl-Bareis, M., Dirnagl, U., 2010. Neurovascular coupling in rat brain operates independent of hemoglobin deoxygenation. J. Cereb. Blood Flow Metab. 30, 757–768.

Logothetis, N.K., 2002. The neural basis of the blood–oxygen-level-dependent functional magnetic resonance imaging signal. Philos. Trans. R. Soc. Lond. Ser. B Biol. Sci. 357, 1003 (ST—The neural basis of the blood–oxygen-le).

Logothetis, N.K., 2008. What we can do and what we cannot do with fMRI. Nature 453, 869–878.

Logothetis, N.K., Wandell, B.a., 2004. Interpreting the BOLD signal. Annu. Rev. Physiol. 66, 735–769.

Lu, H., Golay, X., Pekar, J.J., Van Zijl, P.C.M., 2004. Sustained poststimulus elevation in cerebral oxygen utilization after vascular recovery. J. Cereb. Blood Flow Metab. 24, 764–770.

Lu, J., Dai, G., Egi, Y., Huang, S., Kwon, S.J., Lo, E.H., Kim, Y.R., 2009. Characterization of cerebrovascular responses to hyperoxia and hypercapnia using MRI in rat. NeuroImage 45, 1126–1134.

Mandeville, J.B., Marota, J.J., Kosofsky, B.E., Keltner, J.R., Weissleder, R., Rosen, B.R., Weisskoff, R.M., 1998. Dynamic functional imaging of relative cerebral blood volume during rat forepaw stimulation. Magn. Reson. Med. 39, 615–624.

Markram, H., Toledo-Rodriguez, M., Wang, Y., Gupta, A., Silberberg, G., Wu, C., 2004. Interneurons of the neocortical inhibitory system. Nat. Rev. Neurosci. 5, 793–807.

Marreiros, A.C., Kiebel, S.J., Friston, K.J., 2008. Dynamic causal modelling for fMRI: a two-state model. NeuroImage 39, 269–278 (ST — Dynamic causal modelling for fMRI: a).

Masamoto, K., Kanno, I., 2012. Anesthesia and the quantitative evaluation of neurovascular coupling. J. Cereb. Blood Flow Metab. 32, 1233–1247.

Masamoto, K., Vazquez, A., Wang, P., Kim, S.-G., 2008. Trial-by-trial relationship between neural activity, oxygen consumption, and blood flow responses. NeuroImage 40, 442–450.

Mayhew, S.D., Mullinger, K.J., Bagshaw, a.P., Bowtell, R., Francis, S.T., 2014. Investigating intrinsic connectivity networks using simultaneous BOLD and CBF measurements. NeuroImage 99, 111–121.

Miller, K.L., Luh, W.M., Liu, T.T., Martinez, A., Obata, T., Wong, E.C., Frank, L.R., Buxton, R.B., 2001. Nonlinear temporal dynamics of the cerebral blood flow response. Hum. Brain Mapp. 13, 1–12 (ST — Nonlinear temporal dynamics of the cere.).

Morris, K.F., Nuding, S.C., Segers, L.S., Baekey, D.M., Shannon, R., Lindsey, B.G., Dick, T.E., 2010. Respiratory and Mayer wave-related discharge patterns of raphé and pontine neurons change with vagotomy. J. Appl. Physiol. 109, 189–202.

Mullinger, K.J., Mayhew, S.D., Bagshaw, A.P., Bowtell, R., Francis, S.T., 2013. Poststimulus undershoots in cerebral blood fl ow and BOLD fMRI responses are modulated by poststimulus neuronal activity.

Mullinger, K.J., Mayhew, S.D., Bagshaw, a.P., Bowtell, R., Francis, S.T., 2014. Evidence that the negative BOLD response is neuronal in origin: a simultaneous EEG-BOLD-CBF study in humans. NeuroImage 94, 263–274.

Nagaoka, T., Zhao, F., Wang, P., Harel, N., Kennan, R.P., Ogawa, S., Kim, S.-G., 2006. Increases in oxygen consumption without cerebral blood volume change during visual stimulation under hypotension condition. J. Cereb. Blood Flow Metab. 26, 1043–1051.

Obata, T., Liu, T.T., Miller, K.L., Luh, W.M., Wong, E.C., Frank, L.R., Buxton, R.B., 2004. Discrepancies between BOLD and flow dynamics in primary and supplementary motor areas: application of the balloon model to the interpretation of BOLD transients. NeuroImage 21, 144–153 (ST — Discrepancies between BOLD and flow.).

Ozaki, T., 1992. A bridge between nonlinear time series models and nonlinear stochastic dynamical systems: a local linearization approach. Stat. Sin. 2, 113–135 (ST — A bridge between nonlinear time ser.).

Penny, W.D., Stephan, K.E., Daunizeau, J., Rosa, M.J., Friston, K.J., Schofield, T.M., Leff, A.P., 2010. Comparing families of dynamic causal models. PLoS Comput. Biol. 6 (e1000709-e1000709).

Powers, J., Hirsch, I.R.L.B., Cryer, E., Hirsch, I.B., Cryer, E., 1996. Effect of stepped hypoglycemia flow response to physiological on regional cerebral brain activation blood ∗ O-r. Am. J. Physiol. 270, 5.

Ress, D., Thompson, J.K., Rokers, B., Khan, R.K., Huk, A.C., 2009. A model for transient oxygen delivery in cerebral cortex. Front. Neuroenerg. 1, 3-3.

Riera, J.J., Sumiyoshi, A., 2010. Brain oscillations: ideal scenery to understand the neurovascular coupling. Curr. Opin. Neurol. 23, 374–381.

Roebroeck, A., Formisano, E., Goebel, R., 2011. The identification of interacting networks in the brain using fMRI: Model selection, causality and deconvolution. NeuroImage 58, 6.

Rostrup, E., Knudsen, G.M., Law, I., Holm, S., Larsson, H.B.W., Paulson, O.B., 2005. The relationship between cerebral blood flow and volume in humans. NeuroImage 24, 1–11.

Sadaghiani, S., Uğurbil, K., Uludağ, K., 2009. Neural activity-induced modulation of BOLD poststimulus undershoot independent of the positive signal. Magn. Reson. Imaging 27, 1030–1038.

Sheth, S.a., Nemoto, M., Guiou, M., Walker, M., Pouratian, N., Toga, A.W., 2004. Linear and nonlinear relationships between neuronal activity, oxygen metabolism, and hemodynamic responses. Neuron 42, 347–355.

Shmuel, A., Augath, M., Oeltermann, A., Logothetis, N.K., 2006. Negative functional MRI response correlates with decreases in neuronal activity in monkey visual area V1. Nat. Neurosci. 9, 569–577.

Sotero, R.C., Trujillo-Barreto, N.J., 2007. Modelling the role of excitatory and inhibitory neuronal activity in the generation of the BOLD signal. NeuroImage 35, 149–165 (ST — Modelling the role of excitatory and.).

Stephan, K.E., Weiskopf, N., Drysdale, P.M., Robinson, P.A., Friston, K.J., 2007. Comparing hemodynamic models with DCM. NeuroImage 38, 387–401 (ST — Comparing hemodynamic models with DC.).

Stephan, K.E., Kasper, L., Harrison, L.M., Daunizeau, J., den Ouden, H.E.M., Breakspear, M., Friston, K.J., 2008. Nonlinear dynamic causal models for fMRI. NeuroImage 42, 649–662.

Takano, T., Tian, G.-F., Peng, W., Lou, N., Libionka, W., Han, X., Nedergaard, M., 2006. Astrocyte-mediated control of cerebral blood flow. Nat. Neurosci. 9, 260–267.

Uludağ, K., Dubowitz, D.J., Yoder, E.J., Restom, K., Liu, T.T., Buxton, R.B., 2004. Coupling of cerebral blood flow and oxygen consumption during physiological activation and deactivation measured with fMRI. NeuroImage 23, 148–155.

Uludağ, K., Müller-Bierl, B., Uğurbil, K., 2009. An integrative model for neuronal activity-induced signal changes for gradient and spin echo functional imaging. NeuroImage 48, 150–165.

Valdes-Sosa, P.a., Roebroeck, A., Daunizeau, J., Friston, K., 2011. Effective connectivity: influence, causality and biophysical modeling. NeuroImage 58, 339–361.

van Raaij, M.E., Lindvere, L., Dorr, A., He, J., Sahota, B., Foster, F.S., Stefanovic, B., 2012. Quantification of blood flow and volume in arterioles and venules of the rat cerebral cortex using functional micro-ultrasound. NeuroImage 63, 1030–1037.

van Zijl, P.C.M., Hua, J., Lu, H., 2012. The BOLD post-stimulus undershoot, one of the most debated issues in fMRI. NeuroImage 62, 1092–1102.

Vanzetta, I., Hildesheim, R., Grinvald, A., 2005. Compartment-resolved imaging of activity-dependent dynamics of cortical blood volume and oximetry. J. Neurosci. Off. J. Soc. Neurosci. 25, 2233–2244.

Vazquez, A.L., Fukuda, M., Kim, S.-G., 2012. Evolution of the dynamic changes in functional cerebral oxidative metabolism from tissue mitochondria to blood oxygen. J. Cereb. Blood Flow Metab. 32, 745–758.

Yeşilyurt, B., Whittingstall, K., Uğurbil, K., Logothetis, N.K., Uludağ, K., 2010. Relationship of the BOLD signal with VEP for ultrashort duration visual stimuli (0.1 to 5 ms) in humans. J. Cereb. Blood Flow Metab. 30, 449–458.

Zappe, A.C., Uludağ, K., Logothetis, N.K., 2008a. Direct measurement of oxygen extraction with fMRI using 6% CO_2 inhalation. Magn. Reson. Imaging 26, 961–967.

Zappe, a.C., Uludağ, K., Oeltermann, a., Uğurbil, K., Logothetis, N.K., 2008b. The influence of moderate hypercapnia on neural activity in the anesthetized nonhuman primate. Cereb. Cortex 18, 2666–2673.

Zonta, M., Angulo, M.C., Gobbo, S., Rosengarten, B., Hossmann, K.-A., Pozzan, T., Carmignoto, G., 2003. Neuron-to-astrocyte signaling is central to the dynamic control of brain microcirculation. Nat. Neurosci. 6, 43–50.